

**UNIVERSIDADE FEDERAL DO PAMPA**

**DANIEL LIMA LEMES**

**A STUDY OF BEAMFORMING AND BEAMSHAPING TECHNIQUES FOR  
UNIFORMLY AND NON-UNIFORMLY SPACED ARRAYS**

**Alegrete**

**2018**



**DANIEL LIMA LEMES**

**A STUDY OF BEAMFORMING AND BEAMSHAPING TECHNIQUES FOR  
UNIFORMLY AND NON-UNIFORMLY SPACED ARRAYS**

A master thesis presented to the Graduate Program in Electrical Engineering of Universidade Federal do Pampa (unipampa, RS) in partial fulfillment of the requirements for the degree of Master in Electrical Engineering in the major subject of Systems of Energy.

Thesis advisor Prof. Dr. Marcos Vinício Thomas Heckler

Thesis co-advisor Dr. Lukasz A. Greda

**Alegrete**

**2018**

Ficha catalográfica elaborada automaticamente com os dados fornecidos  
pelo(a) autor(a) através do Módulo de Biblioteca do  
Sistema GURI (Gestão Unificada de Recursos Institucionais) .

L552s Lemes, Daniel Lima

A study of beamforming and beamshaping techniques for  
uniformly and non-uniformly spaced arrays / Daniel Lima Lemes.  
95 p.

Dissertação(Mestrado)-- Universidade Federal do Pampa,  
MESTRADO EM ENGENHARIA ELÉTRICA, 2018.

"Orientação: Marcos Vinício Thomas Heckler".

1. Rede de Antenas. 2. PSO. 3. Método Taguchi. 4. Antenas  
não-uniformemente espaçadas. 5. Transmissor. I. Título.

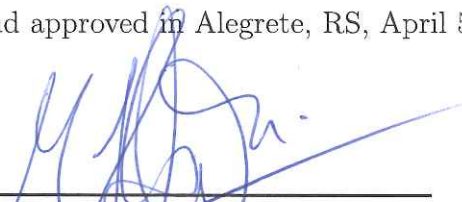


**Daniel Lima Lemes**

**A study of beamforming and beamshaping techniques for  
uniformly and non-uniformly spaced arrays**

A master thesis presented to the Graduate Program in Electrical Engineering of Universidade Federal do Pampa (unipampa, RS) in partial fulfillment of the requirements for the degree of Master in Electrical Engineering in the major subject of Systems of Energy.

Master thesis presented and approved in Alegrete, RS, April 5th. 2018:



---

**Prof. Dr. Marcos Vinício Thomas  
Heckler**  
Advisor



---

**Prof. Dr. Daniel Chagas do  
Nascimento**



---

**Prof. Dr. Djeisson Hoffmann Thomas**

Alegrete, RS  
April 5th, 2018



---

*This work is dedicated to my family and girlfriend for their love and endless support.*



## **ACKNOWLEDGMENTS**

Firstly, I would like to thank my family and my girlfriend for all support, without their support it would not be possible for me to climb this huge mountain.

I also want to thank my advisor Prof. Dr. Marcos V. T. Heckler, who during this time gave his best to teach me not only technical issues but, with examples, he taught me many things that I will carry with me forever. Thank you for the opportunity to travel abroad as well.

Another important part of this work was my colleges of the laboratory LEMA (laboratory of electromagnetics, microwave, and antennas) specially Eduardo Yoshimoto and Juner Vieira. You always were ready to help me, I really appreciate that.

Last but not least, I want to thank the people from DLR (German Aerospace Center), where this work was partially developed specially Dr. Lukasz A. Greda and Andreas Winterstein.

From the deep of my heart, thank you all. This work would not be possible without your help.



*"If you want to go fast, go alone.  
If you want to go far, go together.  
(AFRICAN PROVERB)*





## ABSTRACT

The main goal of this work was to develop a MATLAB-based code capable of finding the optimum values for amplitudes, phases and spacings of a non-uniformly spaced linear antenna array for a specified purpose. This tool allowed investigating the influence of the relative spacings between the elements of an antenna array in its radiation pattern.

Two optimization methods were implemented: PSO (Particle swarm optimization), which is an evolutionary heuristic based on the social interaction and movement of swarms, and Taguchi's method, which is based on orthogonal arrays to reduce the number of experiments needed to find the optimum value of a given variable. Different optimization goals were investigated, so that a comparison between these techniques has been done.

The developed code was applied to solve two practical problems. In the first one, a dual-band antenna array for base stations of mobile communication systems was modeled and its amplitudes, phases and spacings were optimized. By doing so, it was possible to mitigate the grating lobes that appeared in the pattern in the higher band, because the relative spacings between the elements could not be smaller than  $\lambda_0$ . The pattern of this array was also shaped following a squared cosecant contour, in order to illuminate a pico-cell with uniform power. The results of the optimizations in both bands were validated using the commercial software Ansys HFSS and a study about the influence of the mutual coupling in the pattern was done.

The second practical problem was to design an antenna array with beamshaping. By using the proposed code, it was possible to reduce the number of array elements from seven to four comparing to an uniformly spaced array. The optimization was split into two parts in order to mitigate the influence of the mutual coupling. A passive feeder for the optimized array was designed and a prototype was manufactured. The results were validated using HFSS and by measurements. The complete development of the array and of the feeder are detailed in this work.

Finally, the design of a transmitter for adaptive beamshaping is described. The architecture is capable to change the phase and power level of the signal, hence allowing to deliver the weights optimized by the proposed code to the antenna array. A modular concept was chosen in order to increase the flexibility of the transmitter. The device translates the input frequency from 500 MHz to 7 GHz, in order to deliver the weights to the antenna array. Eight transmitters were assembled and they were coupled to the antenna array in order to test their functionality. The patterns were measured in an anechoic chamber. All measured results of the transmitter are presented.

**Key-words:** Antenna array, PSO, Taguchi's method, Non-uniformly spaced antenna arrays, grating lobes, transmitter.



## RESUMO

O principal objetivo deste trabalho foi desenvolver uma ferramenta computacional em MATLAB capaz de otimizar as fases, as amplitudes e os espaçamentos de uma rede de antenas, a fim de satisfazer um determinado objetivo. De posse dessa ferramenta, foi possível analisar a influência do espaçamento relativo entre os elementos de uma rede no diagrama da mesma.

Dois métodos de otimização foram implementados: PSO (*Particle Swarm Optimization*), baseado na interação social e no movimento de um enxame, e o método de *Taguchi*, que utiliza matrizes ortogonais para diminuir o número de testes necessários para otimizar uma variável. Diferentes cenários foram analisados de forma a permitir uma comparação entre os dois métodos.

O código desenvolvido foi aplicado a dois problemas práticos. No primeiro deles, uma rede de antenas dupla-faixa para emprego em estações rádio base de sistemas de comunicações móveis foi modelada e suas amplitudes, fases e espaçamentos foram otimizados. Como na banda mais alta o espaçamento entre os elementos não podia ser menor que  $\lambda_0$ , fez-se necessário otimizar os espaçamentos para controle dos *grating lobes*. O diagrama dessa rede foi também conformado seguindo um contorno em cossecante ao quadrado, para iluminar uma certa região com potência uniforme. Os resultados de todas as otimizações em ambas bandas foram validados usando o software Ansys HFSS e um estudo sobre a influência do acoplamento mútuo foi feito.

O segundo caso consistiu na otimização de uma rede de antenas com conformação de feixe. Foi possível diminuir o número de elementos de sete para quatro em comparação a uma rede com elementos uniformemente espaçados. A otimização foi dividida em duas partes para compensar o efeito do acoplamento mútuo. Para a rede otimizada, um sistema alimentador passivo foi desenvolvido e um protótipo foi fabricado. Os resultados foram validados com simulações no software comercial Ansys HFSS e, também, por medições. Todo o projeto da rede e do alimentador é detalhado neste trabalho.

Finalmente, o desenvolvimento de um circuito transmissor para *beamshaping* adaptativo é detalhado. Tal sistema é composto por um defasador e um amplificador de ganho variável, com os quais é possível inserir as amplitudes e fases, otimizadas pelo código proposto, em uma rede de antenas. Desenvolveu-se um transmissor modular, a fim de aumentar a flexibilidade do sistema. A frequência de entrada do transmissor é de 500 MHz, que é transladada para 7 GHz antes de ser entregue à rede de antenas. Foram fabricados oito transmissores, os quais foram acoplados a uma rede de antenas para testar suas funcionalidades. Os diagramas de irradiação foram medidos em câmara anecóica. Todo o desenvolvimento e medições de cada componente do transmissor são também mostrados neste trabalho.

**Palavras-chave:** Rede de Antenas, PSO, Método de Taguchi, Antenas não-uniformemente espaçadas, grating lobes, transmissor.

## LIST OF FIGURES

|  |    |
|--|----|
| Fig. 1 – USA frequency spectrum. Modified from (TELECOMMUNICATIONS; COMMERCE, 2003). . . . .                                 | 23 |
| Fig. 2 – Geometry of non-uniformly spaced array. . . . .   | 32 |
| Fig. 3 – Two-port network. (Extracted from (BALANIS, 2005)). . . . .   | 33 |
| Fig. 4 – The PSO principle shown graphically. (Adapted from (ROBINSON; RAHMAT-SAMII, 2004)). . . . .                         | 34 |
| Fig. 5 – Flowchart of PSO (modified from (ROBINSON; RAHMAT-SAMII, 2004)).  | 35 |
| Fig. 6 – Results with mask to control the SLL using PSO. . . . .   | 40 |
| Fig. 7 – Results with mask to control SLL and to insert nulls at $-50^\circ$ and $60^\circ$ using PSO. . . . .               | 41 |
| Fig. 8 – Results with mask to steer the main lobe to $30^\circ$ and to control the SLL using PSO. . . . .                    | 41 |
| Fig. 9 – Results with mask to steer the main lobe to $45^\circ$ and to control the SLL using PSO. . . . .                    | 42 |
| Fig. 10 – Results with mask to flatten the main lobe from $-10^\circ$ to $10^\circ$ using PSO. . . . .                       | 42 |
| Fig. 11 – Results with mask to control the SLL using Taguchi’s Method. . . . .   | 43 |
| Fig. 12 – Results with mask to control SLL and to insert nulls at $-50^\circ$ and $60^\circ$ using Taguchi’s Method. . . . . | 44 |
| Fig. 13 – Results with mask to steer the main lobe to $30^\circ$ and to control the SLL using Taguchi’s Method. . . . .      | 45 |
| Fig. 14 – Results with mask to steer the main lobe to $45^\circ$ and to control the SLL using Taguchi’s Method. . . . .      | 45 |
| Fig. 15 – Results with mask to flatten the main lobe from $-10^\circ$ to $10^\circ$ using Taguchi’s Method. . . . .          | 46 |
| Fig. 16 – Layout of the single element: (a) upper view and (b) front view (It was modified from (FARIAS, 2014)). . . . .     | 48 |
| Fig. 17 – Antenna array with annular elements (FARIAS, 2014) . . . . .   | 48 |
| Fig. 18 – Optimized patterns at 1.9 GHz with the main beam pointing to $0^\circ$ . . . . .                                   | 49 |
| Fig. 19 – Optimized patterns at 0.9 GHz with the main beam pointing to $0^\circ$ . . . . .                                   | 50 |
| Fig. 20 – Comparison using HFSS with amplitudes equal to 1 and all phases equal to 0. . . . .                                | 51 |
| Fig. 21 – Optimized patterns at 1.9 GHz with the main beam shaped as a squared cosecant. . . . .                             | 52 |
| Fig. 22 – Optimized patterns at 0.9 GHz with the main beam shaped as a squared cosecant. . . . .                             | 53 |

|   |    |
|---|----|
| Fig. 23 – Comparison using HFSS for the first case (without tolerance) and the second case (tolerance equal to 2dB). . . . .  | 53 |
| Fig. 24 – Layout of the single element: (a) upper view and (b) front view. . . . .  | 56 |
| Fig. 25 – Optimized patterns with different number of elements. . . . .   | 56 |
| Fig. 26 – Variation of the swarm’s best position ( $g_{best}$ ) by optimization of the amplitudes after 150 iterations. . . . .   | 57 |
| Fig. 27 – Variation of the swarm’s best position ( $g_{best}$ ) by optimization of the spacings between the elements after 150 iterations. . . . .  | 57 |
| Fig. 28 – Variation of the fitness function (error) using different values for the self-confidence ( $c_1$ ) and the trust in the swarm ( $c_2$ ). . . . .  | 58 |
| Fig. 29 – Synthesized patterns using different values for the self-confidence ( $c_1$ ) and the trust in the swarm ( $c_2$ ). . . . .   | 58 |
| Fig. 30 – Comparison between the pattern synthesized with the proposed technique (black curve) and the pattern calculated with HFSS (ANSYS, 2016) (blue curve). The red curve is the mask considered for the optimization. . . . .    | 59 |
| Fig. 31 – The final pattern obtained with the second optimization (with 4 elements) and the pattern obtained by (SCHLOSSER et al., 2016) (with 7 elements). 60  |    |
| Fig. 32 – The design of the proposed feeder split in parts. . . . .   | 61 |
| Fig. 33 – The pattern obtained with the coefficients of PSO, the pattern obtained with the coefficients delivery by the developed feeder and the pattern of the integrated system, all of them calculated with HFSS (ANSYS, 2016). 62 |    |
| Fig. 34 – Upper view of the fabricated splitter. . . . .  | 63 |
| Fig. 35 – Measured and simulated parametric curves of the developed splitter. . . . .   | 63 |
| Fig. 36 – Prototype of the proposed antenna array: (a) upper view and (b) bottom view. . . . .  | 64 |
| Fig. 37 – Setup of measurements. . . . .  | 64 |
| Fig. 38 – Picture of the setup. Highlighted on the right it is the Tx antenna and on the left the proposed antenna array. . . . .   | 65 |
| Fig. 39 – Measured result of the S11 parameter. . . . .   | 65 |
| Fig. 40 – The simulated pattern, measured pattern and pattern by (SCHLOSSER et al., 2013). . . . .  | 66 |
| Fig. 41 – Old Version downscaled designed by (MAGALHAES, 2017) . . . . .  | 68 |
| Fig. 42 – First layout designed in this work. . . . .   | 68 |
| Fig. 43 – The schematic of the amplifiers at 1.9 GHz. . . . .   | 69 |
| Fig. 44 – S-parameters for different sets of capacitors and inductors. . . . .  | 69 |
| Fig. 45 – Second layout designed in this work. Without FPC and mixers place correctly. . . . .  | 69 |
| Fig. 46 – Insertion of vias and inductor (L3) soldered directly on the 50 $\Omega$ line . . . . .   | 70 |

|  |    |
|--|----|
| Fig. 47 – Block diagrams of the two transmitter modules: (a) Beamforming unit composed of a mixer, a bandpass filter, a phase shifter and a VGA; (b) Upconverter stage composed of mixer, highpass filter and amplifier. . . . | 71 |
| Fig. 48 – Assembled beamforming (a) and upconverter (b) PCB. The dimensions are 110 mmx36 mm and 74 mmx36 mm, respectively. . . . .  | 72 |
| Fig. 49 – Setup to measure the whole transmitter with a VNA. . . . .   | 73 |
| Fig. 50 – Gain variation for 3 prototypes of the beamforming module. . . . .   | 74 |
| Fig. 51 – S11 and VC21 for 3 prototypes of the upconverter module. . . . .   | 75 |
| Fig. 52 – Measured gain values for the beamforming module. . . . .   | 75 |
| Fig. 53 – Measured phase values for the beamforming module. . . . .  | 76 |
| Fig. 54 – Phase shift introduced by the VGA for different gain values. . . . .   | 76 |
| Fig. 55 – Different insertion loss introduced by the PS for different phase values. . .  | 77 |
| Fig. 56 – Total gain for the complete transmitter controlled by the VGA less the losses introduced by the mixers. . . . .  | 78 |
| Fig. 57 – Total phase shift for the complete transmitter controlled by the phase-shifter.  | 78 |
| Fig. 58 – Tests of eight channels of the proposed transmitter topology (Picture by Andreas Winterstein). . . . .   | 79 |
| Fig. 59 – Picture of the prototype of the antenna used: (a) Upper view; (b) Bottom view. . . . .   | 80 |
| Fig. 60 – Proposed transmitter connection with an eight-element antenna array (Picture by Andreas Winterstein). . . . .  | 80 |
| Fig. 61 – Picture of all system being measured in the anechoic chamber: (a) Without the absorbers; (b) With the absorbers. (Picture by Andreas Winterstein)  | 81 |
| Fig. 62 – Measured radiation patterns obtained with the proposed transmitter architecture of three beamsteering cases with SLL control. . . . .  | 82 |
| Fig. 63 – Measured radiation patterns obtained with the proposed transmitter architecture by digital beamforming. . . . .  | 83 |
| Fig. 64 – An example of mask where from $-180^\circ$ to $-6^\circ$ and from $78^\circ$ to $180^\circ$ the pattern must be below the mask and from $8^\circ$ to $77^\circ$ it must follow the mask.                             | 92 |
| Fig. 65 – Flowchart used for the implementation of both optimization techniques. .   | 94 |

## LIST OF TABLES

|          |   |    |
|----------|---|----|
| Table 1  | – Table extracted from (WENG; YANG; ELSHERBENI, 2007). It shows an OA with 10 parameters, 3 levels, and 27 experiments. The fitness value is also shown . . . . . | 37 |
| Table 2  | – Response table extracted from (WENG; YANG; ELSHERBENI, 2007). It shows the SNR average of each level. . . . .   | 38 |
| Table 3  | – Inter-element spacings for the optimized dual-band antenna array. . . . .   | 50 |
| Table 4  | – Excitation coefficients for radiation in the boresight with suppression of grating and side lobes. . . . .  | 54 |
| Table 5  | – Excitation coefficients for the main beam with squared-cosecant shape. . . . .  | 54 |
| Table 6  | – Center-to-center spacings found by the first optimization . . . . .   | 59 |
| Table 7  | – Normalized Amplitude and Phases of each antenna found after the second optimization . . . . .   | 60 |
| Table 8  | – Input impedances of each antenna taking into account the mutual coupling. 61  |    |
| Table 9  | – Input impedances of each antenna taking into account the mutual coupling. 61  |    |
| Table 10 | – Combined Link Budget . . . . .  | 72 |
| Table 11 | – Prices of Additional Parts . . . . .  | 73 |
| Table 12 | – Coefficients of different steer angles calculated using PSO. . . . .  | 82 |
| Table 13 | – Coefficients of cosecant squared beamshaping calculated using PSO. . . . .  | 83 |



## ABBREVIATIONS

AF – Array factor

DoA – Direction-of-arrival

DoF – Dregrees of freedon

DSRC – Dedicated short range communications

FPC – Fixed-pitch compliant

FPGA – Field-programmable gate array

GA – Genetic algorithm

GSM – Global System for mobile communications

HFSS – High frequency structure simulator

LD – Level difference

LO – Local oscillator

LTE – Long term evolution

MATLAB – Matrix laboratory

MC – Mutual coupling

MSMM – Multiple sweep method of moments

NPSO – Novel particle swarm optimization

NULA – Non-uniformly spaced linear array

OA – Orthogonal array

PCB – Printed circuit board

PS – Phase shifter

PSO – Particle swarm optimization

SINR – Signal-to-interference-and-noise-ratio

SLL – Side lobe level

ULA – Uniform linear array

VGA – Variable gain amplifier

VMC – Vector-mixer calibration

VNA – Vector network analyzer

# CONTENTS

|       |   |    |
|-------|---|----|
|       | Introduction . . . . .  | 23 |
| 1     | STATE-OF-THE-ART OF NON-UNIFORMLY SPACED ARRAYS<br>AND OPTIMIZATION METHODS . . . . .                         | 27 |
| 2     | THEORETICAL BACKGROUND . . . . .  | 31 |
| 2.1   | Antenna Array Theory . . . . .  | 31 |
| 2.2   | Particle Swarm Optimization Method - PSO . . . . .  | 33 |
| 2.3   | Taguchi's Method . . . . .  | 36 |
| 3     | NUMERICAL RESULTS . . . . .   | 39 |
| 3.1   | Numerical Investigations Using PSO . . . . .  | 39 |
| 3.2   | Numerical Investigations Using Taguchi's Method . . . . .   | 43 |
| 3.3   | Comparison of Taguchi's and PSO algorithms . . . . .  | 44 |
| 4     | OPTIMIZATION OF A DUAL-BAND NON-UNIFORMLY SPA-<br>CED ARRAY FOR MOBILE COMMUNICATIONS . . . . .               | 47 |
| 4.1   | Optimization for the main beam pointing to boresight . . . . .  | 47 |
| 4.2   | Optimization for the main beam with squared cosecant shape . . . . .  | 51 |
| 4.3   | Design procedure for arrays composed of dual-band dual-port an-<br>tennas with well separated bands . . . . . | 52 |
| 5     | NON-UNIFORMLY SPACED ARRAYS FOR BEAMSHAPING WITH<br>REDUCED NUMBER OF ELEMENTS . . . . .                      | 55 |
| 5.1   | Application of the PSO for the proposed problem . . . . .   | 55 |
| 5.2   | Feeder Design . . . . .   | 59 |
| 5.2.1 | Fabrication of the designed array . . . . .   | 62 |
| 5.2.2 | Experimental validation of the designed array . . . . .   | 63 |
| 5.3   | Procedure for the design of non-uniformly spaced arrays . . . . .   | 64 |
| 6     | DEVELOPMENT OF TRANSMITTER CIRCUITRY FOR ADAP-<br>TIVE BEAMFORMING . . . . .                                  | 67 |
| 6.1   | Overview of the Design . . . . .  | 67 |
| 6.2   | Final design . . . . .  | 70 |
| 6.3   | Fabricated prototypes . . . . .   | 71 |
| 6.4   | Test and Measurement Methodology . . . . .  | 73 |
| 6.5   | Measurement Results and Performance . . . . .   | 74 |

|       |   |           |
|-------|---|-----------|
| 6.5.1 | Beamforming module . . . . .  | 74        |
| 6.5.2 | Upconverter module . . . . .  | 77        |
| 6.5.3 | Combined Transmitter . . . . .  | 77        |
| 6.6   | Measured patterns . . . . .   | 78        |
| 6.6.1 | Beamsteering using the proposed transmitters . . . . .                              | 79        |
| 6.6.2 | Beamshaping using the proposed transmitters . . . . .                               | 82        |
|       | Conclusion . . . . .  | 85        |
|       | Bibliography . . . . .  | 87        |
|       | <b>Appendix</b>   | <b>89</b> |
| A     | – <b>IMPLEMENTATION ISSUES OF THE STUDIED OPTIMIZATION<br/>TECHNIQUES . . . . .</b> | <b>91</b> |
| A.1   | Setting up the Mask . . . . .   | 91        |
| A.2   | Implementation issues of the Optimization routines . . . . .                        | 92        |

## INTRODUCTION

By analyzing the evolution of frequency allocation in the spectrum, one can notice that there is a large increase in the number of services available. For example, in 1940, the spectrum in the United States was basically divided into 5 bands (COMMISSION, 1940): the band below 100 kHz was occupied by government and commercial long wave fixed service stations; the region from 100 to 200 kHz was allocated for government and maritime traffic, coast and fixed service stations; from 200 to 400 kHz, the band was reserved for government aids to navigation; from 400 to 550 kHz, maritime services were supposed to operate; the rest of the spectrum was allocated for other applications as experimental television system, police issues, amateur radio, among others. In 2003, the spectrum was divided into about 378 bands and cover frequencies from 3 kHz to 300 GHz as shown in Fig. 1

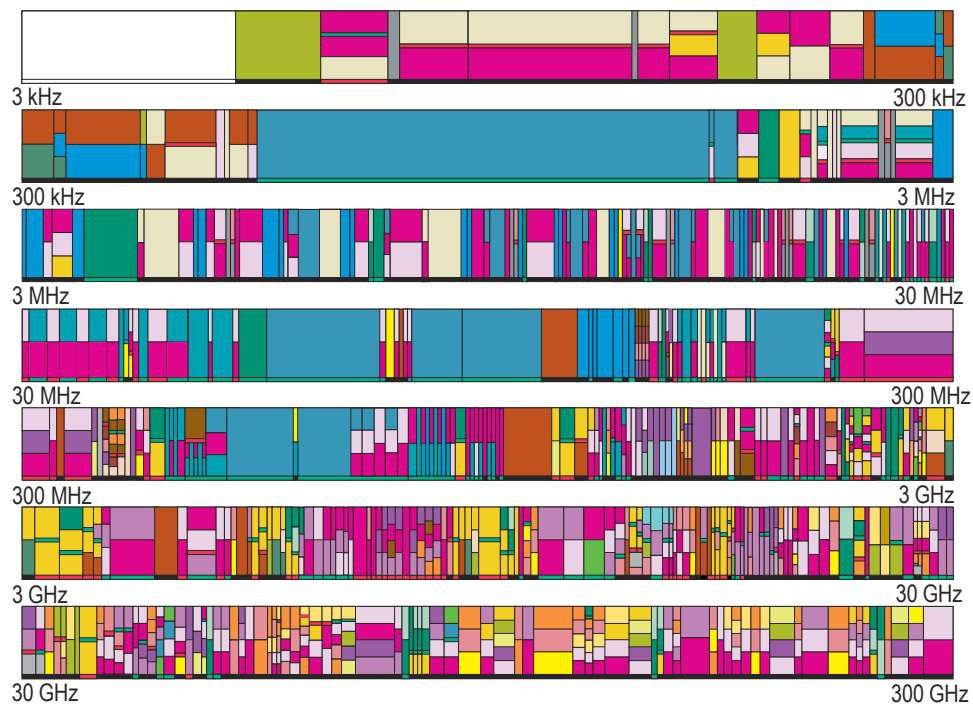


Fig. 1: USA frequency spectrum. Modified from (TELECOMMUNICATIONS; COMMERCE, 2003).

This increase in the number of services brought significant changes to the field of antennas. Nowadays, there are many interference sources and other problems related to this topic. Thus, the antennas need to have their performance increased.

Usually, a single element provides low values of directivity (gain) and it is not possible to change substantially its radiation characteristics, such as, to insert nulls, to shape the beam or to steer the main lobe electronically. These modifications are, sometimes,

necessary to mitigate the problems that appear from the increase in the number of wireless services. Electronic control of the radiation properties are mostly achieved by considering antenna arrays. In an array of identical elements, there are five parameters that can be used to control the pattern, namely the geometrical configuration of the array (linear, circular, rectangular, etc), the relative spacing between the elements, the amplitudes and the phases of the currents imposed at each element, and the individual element pattern (BALANIS, 2005).

There are several papers that deal with the control of amplitudes and phases of each element in an array, in order to modify its radiation pattern. However, there are few studies on the potential of optimizing the inter-element spacing, since uniform spacing between the elements is easier to model and it is the standard case in most applications. The antenna array that has different inter-element spacings is called non-uniformly spaced array. The drawback of such a structure is to find the optimum values of these parameters, because there are many possible combinations.

In order to propose a solution for this problem, many optimization methods can be applied. Two of them will be described and their implementation will be detailed in the next sections. The Particle swarm optimization (PSO) is an evolutionary heuristic based on the social interaction and movement of swarms. The Taguchi's method is based on the concept of orthogonal arrays (OA), which reduce the number of tests required to find the optimum value of a variable for a given problem.

In the following chapter, the state-of-the-art will be presented, where, despite the literature has poorly explored the non-uniformly spaced arrays with beamshaping, some papers with several other goals will be cited in order to show the several possibilities allowed by such structures. After that, the theoretical background will be shown which has the information needed to implement the two optimization methods and to analyze the results.

Then, some numerical results and a comparison between both optimizations methods will be shown. In this chapter, some general conclusion about the optimization of amplitudes, phases and inter-element spacings of an antenna array and the permutation between them, also, will be shown.

The implemented method were applied in two practical problem and the results will be shown. The first problem deals with the optimization of dual-band non-uniformly spaced array for mobile communications in order to mitigate the grating lobes and to shape the main beam following the squared cosecant contour to illuminated a pico-cell with uniform power.

The second one is, also, the optimization of a non-uniformly spaced antenna array but to reduce the number of elements needed. A comparison between the found structure

and a uniformly spaced array is shown. It was developed a passive feeder for the proposed array and the results were validated by simulation and measurements.

Then, the development of an adaptive transmitter which can perform analog and digital beamforming will be pointed out. It will be shown all measured results and, also, a overview of the project. By doing this, it is possible to know some difficulties faced during the process of development and the strategies applied to mitigate that.

Finally, some conclusions about all work will be shown where the results will be briefly commented taking into account all accomplishments of this work.





## 1 STATE-OF-THE-ART OF NON-UNIFORMLY SPACED ARRAYS AND OPTIMIZATION METHODS

Although it is poorly reported in the literature, there are many applications where non-uniformly spaced antenna arrays can be applied. The author in (ATHLEY, 2001) presents a new technique of optimization that is applied to find the best positions of the elements in an antenna array in order to get the best direction-of-arrival (DoA) estimation. Since the DoA estimation accuracy is critically dependent upon the electrical array size, a good way to improve it is by using non-uniformly spaced arrays. By changing the relative spacing between the elements, it is possible to increase the equivalent aperture of the array without increasing the number of elements.

Following the same idea, in (HSIAO; LIN; CHEN, 2015), the authors developed an algorithm focused on increasing the number of degrees of freedom (DoF). This implies in more accuracy in the estimation of direction of arrival using a smart antenna, for example. To increase the DoF, the most widely used method is the try-and-error approach, which demands high computation effort. In order to avoid that, the paper presents a  $K$ -level nested array, which means to divide the array into  $K$  sub-arrays with non-uniform spacing. This method allows working with arrays with a reduced number of elements, hence demanding less computational effort.

Another interesting application is to develop broadband antenna arrays. In (QI-LI; CHAO, 2010) the authors developed a broadband non-uniformly spaced linear array (NULA) combining the Dole's Asymptotic Theory Design technique and an optimization method. The authors started describing the Dole's method as based on the asymptotic theory to calculate the spatial arrangement of the array elements and the magnitude weights to get broadband beams. The main disadvantage of Dole's method is the difficulty to control the beam shape. The authors changed the common array arrangement given by Dole's asymptotic theory by making the array symmetrical to its center. This change was made based on the theory that the resolution performance of non-uniform linear arrays is better with sensors concentrated in the middle of the array. A comparison between the method proposed and Dole's method was done for the same number of elements.

The concept of non-uniformly spaced arrays can be applied also to maximize the Signal-to-Interference-and-Noise Ratio (SINR). In (AL-KA'BI; BIALKOWSKI; HOMER, 2005), the authors concluded that, in the case of uniformly spaced arrays, the SINR is larger than 0 dB when a pointing error of up to  $7.3^\circ$  exists, while, in the case of non-uniformly spaced arrays, positive SINR exists when it has a pointing error up to  $11.3^\circ$ .

The authors in (VARUM; MATOS; ABREU, 2014) developed a non-uniformly receiving array for using at Dedicated Short Range Communications (DSRC). This tech-

nology is used to exchange real time information among vehicles and between vehicles and infrastructure. The proposed array has four elements at the corners with a fifth element at the center. No algorithm has been used to optimize the excitations and the positions of the radiators in the array. However, the authors analyzed the array as an approximation to a binomial configuration, looking at the array as two linear arrays with three elements, being the central element shared by both linear arrays. By doing that, the corner elements are fed with the same amount of power, while the power of the center element is the fourfold. The results are satisfactory according to the standards that regulate this technology, especially because of the non-uniformly relative spacings between the elements.

In (KAWDUNGTA; PHONGCHAROENPANICH; TORRUNGRUENG, 2011), the authors present a method to calculate the current distribution with mutual coupling using the multiple sweep method of moments (MSMM) and the genetic algorithm (GA) to optimize the inter-element spacings in order to minimize the side lobe level. This method was applied to non-uniform spacing collinear dipole antenna arrays in free space and the total field is calculated using the Pocklington's integral equation. The algorithm starts with the initial array parameters, then the MSMM computes the currents of the dipole antennas. After that, a comparison between the radiation pattern estimated and the desired one is made and, if the result is not satisfactory, the GA optimizes the array inter-element spacings. Then, the MSMM calculates again the pattern until the goals are achieved. The results prove that non-uniformly spaced arrays can be used to control the side lobe level in this case.

The paper (STAHRIAN; CHOI; ESHRAGHI, 2009) presents an investigation about beam shaping design using the *minimax algorithm* (JORGENSEN; KAJ, 1981), which is applied to antenna arrays with 148 and 244 non-uniformly spaced elements. Besides that, the paper presents a procedure to match the antenna main lobe to a geographic contour. The array is divided into 3 regions with 3 different relative spacing between the elements.

One of the drawbacks of non-uniformly spaced arrays is the difficulty to find the optimum values for excitation amplitude, relative spacings and phases for each element. One straightforward way is to test all possible combinations of parameters, which is called a *full factorial experiment*. However, in most cases, a lot of time will be spent and this procedure becomes impracticable, specially for arrays with large number of elements. To mitigate this limitation, (ENACHE; POPESCU; DEPARATEANU, 2016) provides a good knowledge about optimization of the space between the elements of a non-uniform linear symmetrical antenna array and their currents. First of all, the currents of the elements are normalized by the current of the first element and the distance between elements are normalized by the wavelength. Then, the authors considered an isotropic radiator, which allows simplifying the radiation equation using the array factor ( $AF$ ). Besides that, they decreased the number of parameters using the linearization that yields only two parameters.

Using genetic algorithm, they found the best solution and applied it to the linearization expression. Some graphics comparing the patterns for uniformly and non-uniformly spaced arrays were shown. However, this technique has been applied just for isotropic elements and symmetrical arrays.

The paper (KAIFAS; BABAS; SAHALOS, 2013) presents a procedure to build a non-uniformly spaced array. First, a deterministic procedure was performed to find the aperture size and the number of elements; then, a stochastic procedure was undertaken to find the element local arrangement. The deterministic approach is based on the use of an aperture with uniformly excited and non-uniformly spaced array. The stochastic approach is mostly based on the use of evolutionary optimization algorithms. This technique is applied for an array with a large number of elements.

In (WENG; YANG; ELSHERBENI, 2007), the authors present a novel optimization technique applied in Electromagnetics that is called as Taguchi's Method. It is based on orthogonal arrays and will be described with more details later.

The authors in (ROBINSON; RAHMAT-SAMII, 2004) describe and apply the particle swarm optimization (PSO) in high-frequency Electromagnetics for the first time. This method is based on the movement of swarms. The particles fly around the search space and their best value and the best global value are recorded in each iteration. After that, the next movement of the particle is updated based on these best values. This method will be also described later in detail.

In order to improve the PSO method so as to obtain the optimum solution in less time, the authors (BARBOSA et al., 2015) introduced one particle with the Dolph-Tschebysheff's weights into the solution space of PSO so as to accelerate convergence. However, since the Dolph-Tschebysheff method requires uniform spacing, it can not be applied for non-uniformly spaced arrays and, therefore has not been considered in this work.



## 2 THEORETICAL BACKGROUND

### 2.1 ANTENNA ARRAY THEORY

For many applications, beamshaping or beamsteering are required, and, to reach these goals an antenna array is necessary, in most of the cases, since it brings more DoF in terms of changing the radiation pattern.

The total field of an antenna array is determined by the vector sum of the fields radiated by the individual elements (BALANIS, 2005). In some cases, depending mainly on the radiation pattern of the element and the inter-element spacings, it is possible to simplify this calculation by considering the radiation pattern of the single and isolated element placed  $N$  times along a line. Then, for a linear array, the total field is given by

$$\vec{E}_{total} = \vec{E}_{single\ element} * (AF). \quad (2.1)$$

The array factor ( $AF$ ) is dependent on the geometry of the array, the separation between the elements, the amplitudes and the excitation phase. For a linear array with equal elements, uniform amplitude distribution and uniformly spaced elements, the  $AF$  is given by

$$AF = \sum_{n=1}^N e^{j(n-1)[kdcos(\gamma)+\beta]}, \quad (2.2)$$

where  $N$  is the number of elements,  $k$  is the wavenumber in free space,  $d$  is the distance between the elements,  $\beta$  is the progressive phase shift and  $cos(\gamma)$  is equal to  $cos(\theta)$ , when the array is along the  $z$ -axis,  $\sin(\theta) \cos(\phi)$ , when the elements are along the  $x$ -axis, or  $\sin(\theta) \sin(\phi)$ , when they are along the  $y$ -axis.

For non-uniformly spaced arrays, which are the main topic of this work, the  $AF$  cannot be found using (2.2). This occurs because the distance between adjacent elements is not constant. This is schematically shown in Fig. 2. Therefore, the general form of  $AF$  must be adapted to

$$AF = \sum_{n=1}^N a_n e^{jk\delta_n \cos(\gamma)} \quad (2.3)$$

where  $a_n$  is the complex weight, which assumes values between 0 and 1 for the amplitude and values between  $0^\circ$  and  $360^\circ$  for phase of the  $n$ -th element and  $\delta_n$  is the position of the  $n$ -th element in the array. These parameters must be optimized by any optimization technique. In this work, the array has been optimized by using PSO and the Taguchi's techniques, which are described in the next sections.

At the same time, even the showed adapted form of  $AF$  is an approximation because it take into account the single and isolated element. When two or more antennas are near

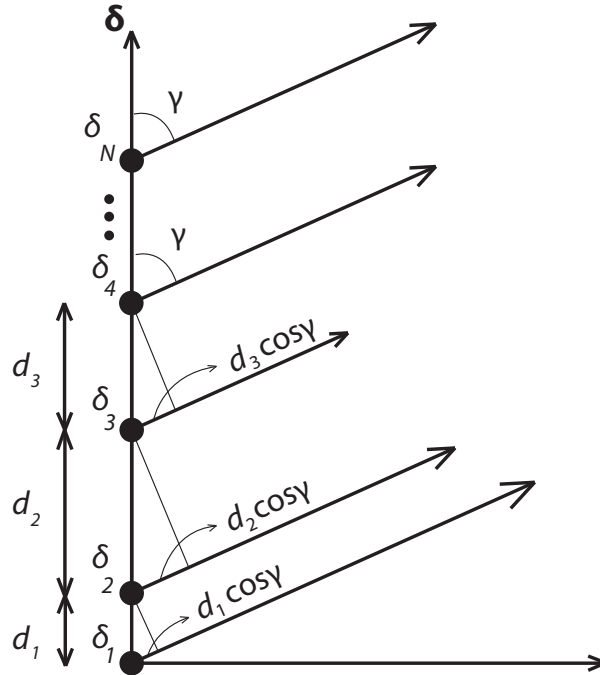


Fig. 2: Geometry of non-uniformly spaced array.

to each other, the energy radiated by one is coupled to the other, i.e. the radiated power of one element induces a current in the others. Thus, the radiation pattern of one element depends not only on its own current but also on the current of neighboring elements. The interchange of energy is known as mutual coupling (BALANIS, 2005). It depends mainly on the inter-element spacings and the radiation characteristics of each element.

Because of the mutual coupling, the total field of an antenna array must take into account the field of each element and it is given by

$$\vec{E}_{\text{total}} = \sum_{n=1}^N \vec{E}_n * a_n e^{jk\delta_n \cos(\gamma)}, \quad (2.4)$$

where  $\vec{E}_n$  is the field of the  $n$ -th array element considering the reference as the center of the  $n$ -th element.

For most configurations, the mutual coupling is difficult to predict analytically. In this work, when convenient, the commercial software Ansys HFSS (ANSYS, 2016) will be used to account for this effect and the radiation pattern of each element will be exported from it. The field exported from HFSS is called active pattern and it is extracted considering the other elements of the array with a  $50\Omega$  load in the input.

An additional effect of the mutual coupling is the modification on the input impedance of the elements. By representing a two-element array as a two-port network, as

shown in Fig. 3, its voltage-current relations is given by

$$\begin{aligned} V_1 &= Z_{11}I_1 + Z_{12}I_2 \\ V_2 &= Z_{21}I_1 + Z_{22}I_2 \end{aligned} \quad (2.5)$$

where

$$Z_{11} = \left. \frac{V_1}{I_1} \right|_{I_2=0}, \quad (2.6)$$

$$Z_{22} = \left. \frac{V_2}{I_2} \right|_{I_1=0}, \quad (2.7)$$

$$Z_{12} = \left. \frac{V_1}{I_2} \right|_{I_1=0}, \quad (2.8)$$

and

$$Z_{21} = \left. \frac{V_2}{I_1} \right|_{I_2=0}. \quad (2.9)$$

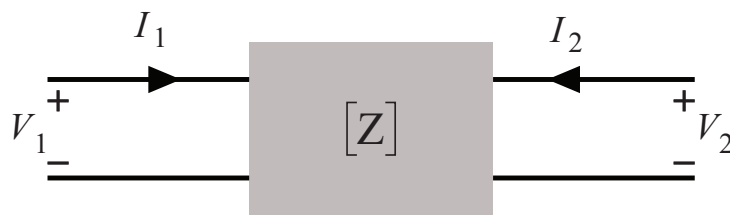


Fig. 3: Two-port network. (Extracted from (BALANIS, 2005)).

By analyzing (2.5), one can see the influence of antenna 1 upon antenna 2 and vice-versa. The parameters  $Z_{12}$  and  $Z_{21}$  are known as mutual impedances. This effect must be taken into account because it modifies the radiation pattern of the antenna array. The quantification of this modification will be shown in the next chapters and also a procedure to mitigate that will be discussed.

## 2.2 PARTICLE SWARM OPTIMIZATION METHOD - PSO

The first work that reported the application of PSO in Electromagnetics is (ROBINSON; RAHMAT-SAMII, 2004). In this paper, the authors describe the technique as “a robust stochastic evolutionary computation technique based on the movement and intelligence of swarms.”

The technique describes a swarm of bees looking for flowers. When a bee finds a place with high density of flowers, this position will be classified as its best position. The bees communicate with each other to know what is the best position among all of them. The next movement of each bee is governed by its best position, by the best position found by the whole swarm and by how much they trust themselves and in the group. After some iterations, the swarm will converge to the same point. In other words, the swarm,

after going through all the metaspace, will find the place that has the highest density of flowers. In terms of optimization, each bee corresponds to a particle. By using these concepts, the movement of the  $i$ -th particle is described mathematically by

$$v_{k,s}^{i-th} = w * v_{k-1,s}^{i-th} + c_1 * rand * (p_{best,s} - x_{k-1,s}) + c_2 * rand * (g_{best,s} - x_{k-1,s}), \quad (2.10)$$

where  $v_{k,s}^{i-th}$  is the speed of the  $i$ -th particle in the  $s$ -th dimension and in the  $k$ -th iteration,  $x_{k-1}$  is the particle's position in the  $(k-1)$ -th iteration,  $w$  is the inertia,  $c_1$  and  $c_2$  are the trust in themselves and in the group, respectively,  $p_{best,s}$  is the best position found by each particle in the  $s$ -th dimension,  $g_{best,s}$  is the best position found by all particles in the  $s$ -th dimension and  $rand$  is a random number. Each dimension represents a variable of the problem that must be optimized. Fig. 4 shows (2.10) graphically, where the bold vector points to the place to be occupied by the bee in the next iteration.

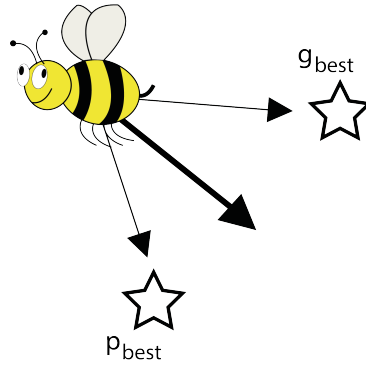


Fig. 4: The PSO principle shown graphically. (Adapted from (ROBINSON; RAHMAT-SAMII, 2004)).

An important issue of optimization is to establish a link between the optimization algorithm and the problem that must be optimized. The fitness function is the responsible to provide this link. Basically the fitness represents, in a single number, the ability to solve the particle's problem. For this work, the fitness function is given by

$$fitness = \sum_{\theta=-90^{\circ}}^{90^{\circ}} \vec{E}_{mask,\theta} - \vec{E}_{calc,\theta}, \quad (2.11)$$

where  $\vec{E}_{mask}$  stands for the mask values and  $\vec{E}_{calc}$  for the calculated pattern using (2.4). The mask is the value of each angle which represents the goal that must be achieved by the optimization. In other words, the fitness function is given by the overall sum of the discrepancies between the mask and the synthesized patterns.

A particularity of the PSO is that the particles are not always confined in the metaspace. Sometimes, the next speed calculated points to a position outside of the metaspace. To mitigate this inconvenient, the authors proposed three different boundary conditions. The first one is the “absorbing wall” where the particle has its speed zeroed





Some improvements in PSO were suggested in the literature. The paper (MALDAL; DAS; BHATTACHARJEE, 2010) presents a novel technique of optimization based on Particle Swarm Optimization technique (NPSO). The technique is demonstrated for the case of arrays composed of isotropic antennas. The standard PSO algorithm deals with two random numbers. If both are small, the personal and social experiences are not used fully and, if both are large, the personal and social experiences are overused and the particle is driven too far away. The NPSO uses just one random number ( $R$ ); then the social and personal experiences are multiplied by  $R$  and  $(1-R)$  respectively. Besides that, a memory is introduced on the equation in order to avoid the worst solutions ( $p_{worst}$ ), so that the particle bypasses the worst positions when it is driven to them.

### 2.3 TAGUCHI'S METHOD

In (WENG; YANG; ELSHERBENI, 2007), the authors reported the application of Taguchi's method to Electromagnetics for the first time. This algorithm is a global optimization technique based on the concept of orthogonal arrays (OA). This is an efficient way to minimize the number of experiments needed to achieve a given optimization. In this method, each column of the OA represents one parameter to be optimized. The authors show that to optimize 10 parameters, where each has three levels, the use of full factorial strategy would yield 59049 experiments, whilst only 27 experiments are needed using Taguchi's method.

According to (WENG; YANG; ELSHERBENI, 2007), three levels are enough to characterize nonlinear effects. The first step of the algorithm is to set them. Level 2 is set as the center of the limits previously set by the user. Levels 1 and 3 are found subtracting/adding the value of level 2 with a parameter called level difference (LD) which can be obtained, for the first iteration, using

$$LD_1 = \frac{max - min}{\text{number of levels} + 1}, \quad (2.12)$$

where  $max$  is the upper limit and  $min$  the under limit of the parameter.

For example, for excitation currents in antenna arrays, the normalization of values is a standard procedure, so that the possible range of values is from 0 to 1. Therefore, level 1 would be equal to 0, level 2 would be 0.5 and level 3 would be 1.0 at the beginning of the optimization.

In each iteration, to reduce the optimization range, the  $LD$  is multiplied with a reduced rate to obtain  $LD_{i+1}$  for the  $(i+1)$ -th iteration. By doing so, the values can be refined until the global minimum is found. After each iteration, a response table (based on the fitness function) is made, and based on that, the method chooses the best value to be set as the second level for the next iteration. The OA makes sure that all levels are in the same number in each row. In order words, this ensures that all combinations are

Table 1: Table extracted from (WENG; YANG; ELSHERBENI, 2007). It shows an OA with 10 parameters, 3 levels, and 27 experiments. The fitness value is also shown

| Experiment / Element | 1 | 2 | 3 | 4 | 5 | 6 | 7 | 8 | 9 | 10 | Fitness | SNR (dB) |
|----------------------|---|---|---|---|---|---|---|---|---|----|---------|----------|
| 1                    | 1 | 1 | 1 | 1 | 1 | 1 | 1 | 1 | 1 | 1  | 5.153   | -14.240  |
| 2                    | 2 | 1 | 2 | 2 | 2 | 3 | 3 | 1 | 2 | 3  | 9.076   | -19.157  |
| 3                    | 3 | 1 | 3 | 3 | 3 | 2 | 2 | 1 | 3 | 2  | 9.578   | -19.625  |
| 4                    | 1 | 2 | 1 | 2 | 2 | 2 | 3 | 3 | 1 | 2  | 9.847   | -19.866  |
| 5                    | 2 | 2 | 2 | 3 | 3 | 1 | 2 | 3 | 2 | 1  | 6.821   | -16.676  |
| 6                    | 3 | 2 | 3 | 1 | 1 | 3 | 1 | 3 | 3 | 3  | 14.233  | -23.066  |
| 7                    | 1 | 3 | 1 | 3 | 3 | 3 | 2 | 2 | 1 | 3  | 12.898  | -22.210  |
| 8                    | 2 | 3 | 2 | 1 | 1 | 2 | 1 | 2 | 2 | 2  | 9.911   | -19.922  |
| 9                    | 3 | 3 | 3 | 2 | 2 | 1 | 3 | 2 | 3 | 1  | 9.073   | -19.155  |
| 10                   | 1 | 1 | 2 | 1 | 2 | 2 | 2 | 3 | 3 | 1  | 9.245   | -19.319  |
| 11                   | 2 | 1 | 3 | 2 | 3 | 1 | 1 | 3 | 1 | 3  | 14.696  | -23.344  |
| 12                   | 3 | 1 | 1 | 3 | 1 | 3 | 3 | 3 | 2 | 2  | 11.785  | -21.427  |
| 13                   | 1 | 2 | 2 | 2 | 3 | 3 | 1 | 2 | 3 | 2  | 7.690   | -17.719  |
| 14                   | 2 | 2 | 3 | 3 | 1 | 2 | 3 | 2 | 1 | 1  | 7.220   | -17.171  |
| 15                   | 3 | 2 | 1 | 1 | 2 | 1 | 2 | 2 | 2 | 3  | 11.447  | -21.174  |
| 16                   | 1 | 3 | 2 | 3 | 1 | 1 | 3 | 1 | 3 | 3  | 12.176  | -21.710  |
| 17                   | 2 | 3 | 3 | 1 | 2 | 3 | 2 | 1 | 1 | 2  | 7.716   | -17.748  |
| 18                   | 3 | 3 | 1 | 2 | 3 | 2 | 1 | 1 | 2 | 1  | 7.553   | -17.563  |
| 19                   | 1 | 1 | 3 | 1 | 3 | 3 | 3 | 2 | 2 | 1  | 10.495  | -20.419  |
| 20                   | 2 | 1 | 1 | 2 | 1 | 2 | 2 | 2 | 3 | 3  | 11.054  | -20.871  |
| 21                   | 3 | 1 | 2 | 3 | 2 | 1 | 1 | 2 | 1 | 2  | 12.142  | -21.686  |
| 22                   | 1 | 2 | 3 | 2 | 1 | 1 | 2 | 1 | 2 | 2  | 10.197  | -20.169  |
| 23                   | 2 | 2 | 1 | 3 | 2 | 3 | 1 | 1 | 3 | 1  | 11.646  | -21.324  |
| 24                   | 3 | 2 | 2 | 1 | 3 | 2 | 3 | 1 | 1 | 3  | 11.940  | -21.540  |
| 25                   | 1 | 3 | 3 | 3 | 2 | 2 | 1 | 3 | 2 | 3  | 11.702  | -21.365  |
| 26                   | 2 | 3 | 1 | 1 | 3 | 1 | 3 | 3 | 3 | 2  | 11.695  | -21.360  |
| 27                   | 3 | 3 | 2 | 2 | 1 | 3 | 2 | 3 | 1 | 1  | 9.354   | -19.420  |

tested. Table 1 shows an example of OA for an problem with 10 variables and also the fitness value of each experiment.

By averaging the SNR values for each parameter, it is possible to build up the response table which is shown in Table 2. Then, by analyzing the values, it is possible to set which level will be the center level in the next iteration, the chosen levels are highlighted in gray.

Table 2: Response table extracted from (WENG; YANG; ELSHERBENI, 2007). It shows the SNR average of each level.

| Level/ Element | 1     | 2     | 3      | 4     | 5     | 6     | 7     | 8     | 9     | 10    |
|----------------|-------|-------|--------|-------|-------|-------|-------|-------|-------|-------|
| 1              | -19.6 | -20.0 | -20.0  | -19.8 | -19.7 | -19.9 | -20.0 | -19.2 | -19.6 | -18.3 |
| 2              | -19.7 | -19.8 | -19.6  | -19.7 | -20.0 | -19.6 | -19.6 | -20.0 | -19.7 | -19.9 |
| 3              | -20.5 | -20.0 | -20.23 | -20.3 | -20.0 | -20.2 | -20.2 | -20.6 | -20.4 | -21.6 |

### 3 NUMERICAL RESULTS

In this chapter, the pattern of the single element proposed by (FARIAS, 2014) was used in order to perform different optimizations and extract general conclusions about the PSO and Taguchi's method. This antenna will be better described in the next chapter where an optimization will be performed to solve a practical problem introduced by this antenna.

These optimizations were also performed to investigate which features the modification on the relative spacings between the elements brings to the pattern. In (BALANIS, 2005), the author states that it is possible to mitigate the grating lobes by modifying the relative spacings. Based on that, some optimizations were performed with spacings larger than  $\lambda_0$  and will be shown in the next chapter.

The investigation was also done in order to find out which parameters must be optimized to achieve a certain goal. Five masks with different optimization goals were created: flat main lobe centered at  $\theta = 0^\circ$ , beam steering to  $30^\circ$  and  $45^\circ$ , insertion of nulls in the pattern and simple control of side lobe level (SLL). For all the 5 masks, a common goal is to control the SLL but as second priority. The following analyses are based on permutations of the three parameters for each element: spacing, phases and amplitudes. When phases were not optimized, they were set to  $0^\circ$  by default. The analyses also show the optimization results using all the three parameters simultaneously. The fitness function was set so as to force the directivity to be above a minimum level. For all optimizations, an array with seven elements was used and the search for relative spacings was allowed in the interval  $0.3\lambda_0 < d < \lambda_0$ .

#### 3.1 NUMERICAL INVESTIGATIONS USING PSO

For all simulations, PSO was set to work with 100 particles, 200 for the maximum number of iterations,  $c_1 = c_2$  and  $w = 0.9$ . The best values for these parameters vary depending on the array and optimization goals.

In Fig. 6, where the goal was to control the SLL and to achieve a minimum level of directivity (at least 8 dBi), the best result was obtained optimizing only the amplitude and the positions of the elements. Optimizing phase and amplitude provided good result in terms of fulfilling the mask, but the difference to the result obtained by optimizing amplitude and spacing is the achieved directivity: 13.5 dBi for the latter and 11.2 dBi for the former. When phase and spacings were optimized (blue curve), the goal was not achieved and it can be explained by the fact that the SLL is mainly controlled by the amplitude distribution. In this case, the optimization of the spacings controlled only partially the SLL.

The optimization of all three variables together did not provide satisfactory results. In order to try obtaining satisfactory results by varying the three parameters, the maximum number of iterations was increased to 1000 and the number of particles to 200. However, even with these modifications, satisfactory results were not achieved. The solution to this is to fine tune the social parameter: by decreasing  $c_2$ , the particles can explore more freely the metaspace and converge to a better place. An investigation about  $c_1$  and  $c_2$  was performed and will be pointed out in section 5.

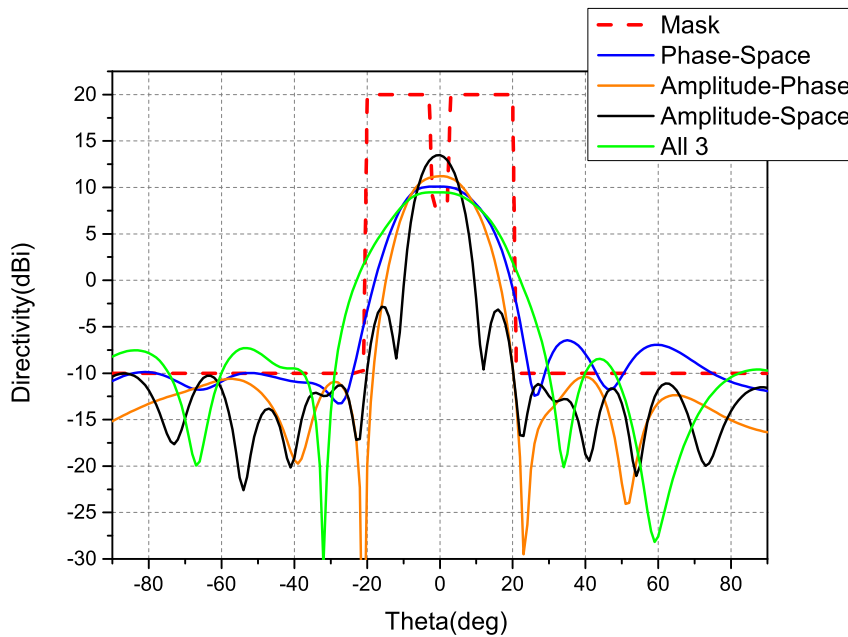


Fig. 6: Results with mask to control the SLL using PSO.

In Fig. 7, nulls at  $\theta = -50^\circ$  and  $\theta = 60^\circ$  were added on the mask whilst the control of SLL and a minimum value of directivity are still required. The worst result is obtained when just phase and spacing were optimized (blue curve). As pointed out before, the amplitude is the main parameter to perform SLL control. All other three optimizations provided good results in terms of fulfilling the mask. Also in this case, the highest gain has been achieved when the amplitude and spacings were optimized. This is due the fact that the gain is proportional to the electrical size of the array and, by optimizing the spacings, effective aperture can be increased.

For Figs. 8 and 9, the optimization of only amplitudes and spacings yielded the worst results. For steering angle equal to  $30^\circ$ , all other combinations achieved good and similar results, whilst, for steering angle equal to  $45^\circ$ , phase and amplitude and all 3 achieved acceptable results. This occurs because, based on (BALANIS, 2005), it is known that phases are mainly responsible to steer the beam.

Fig. 10 shows a mask with beamshaping and control of SLL. This investigation

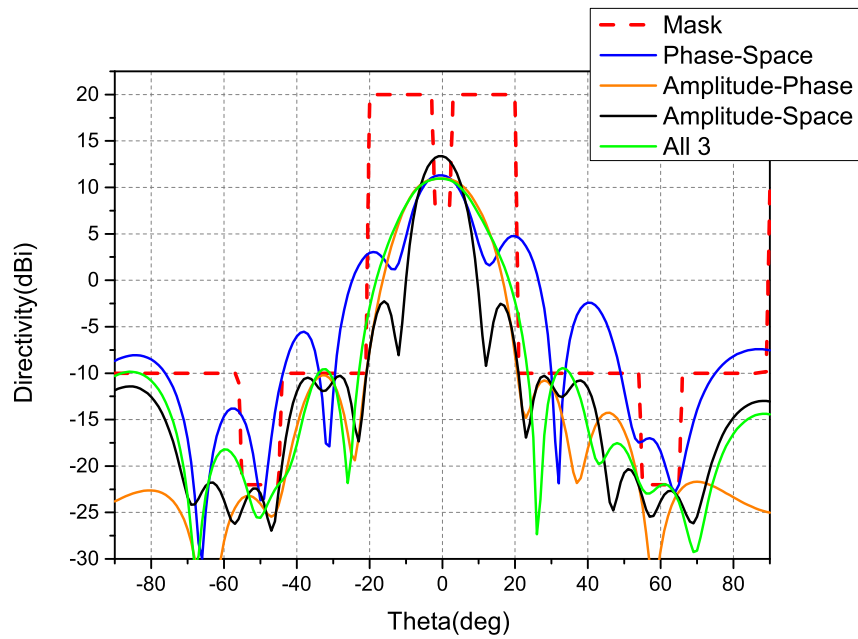


Fig. 7: Results with mask to control SLL and to insert nulls at  $-50^\circ$  and  $60^\circ$  using PSO.

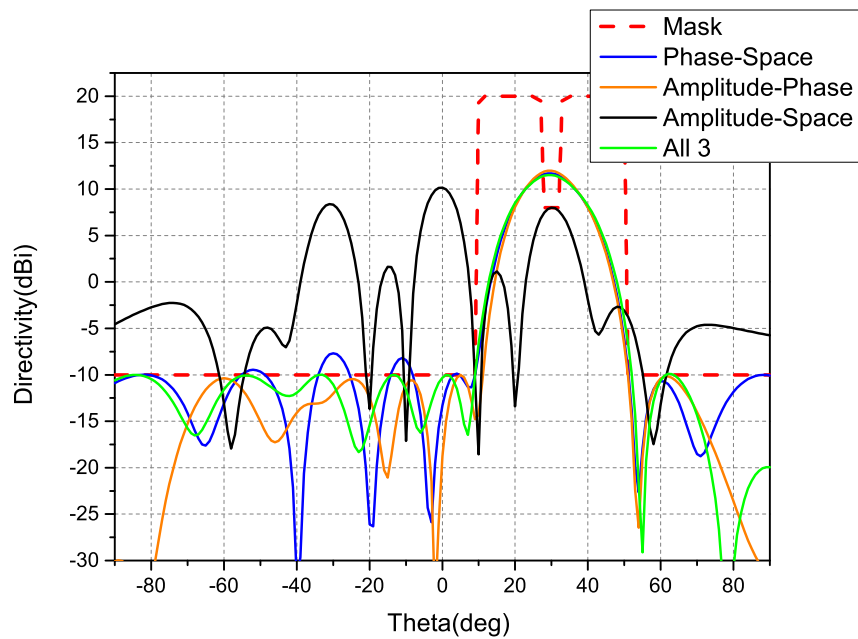


Fig. 8: Results with mask to steer the main lobe to  $30^\circ$  and to control the SLL using PSO.

was done in order to know the capability of the non-uniformly spaced array to shape the main beam. The best result was obtained optimizing all 3 parameters together (green curve). The goal of this mask is to force the pattern to follow the mask from  $-10^\circ$  to  $10^\circ$ . Due to the small number of elements used, the mask has been only partially fulfilled. For beamshaping, the best option is to normalize the pattern in order to exclude the

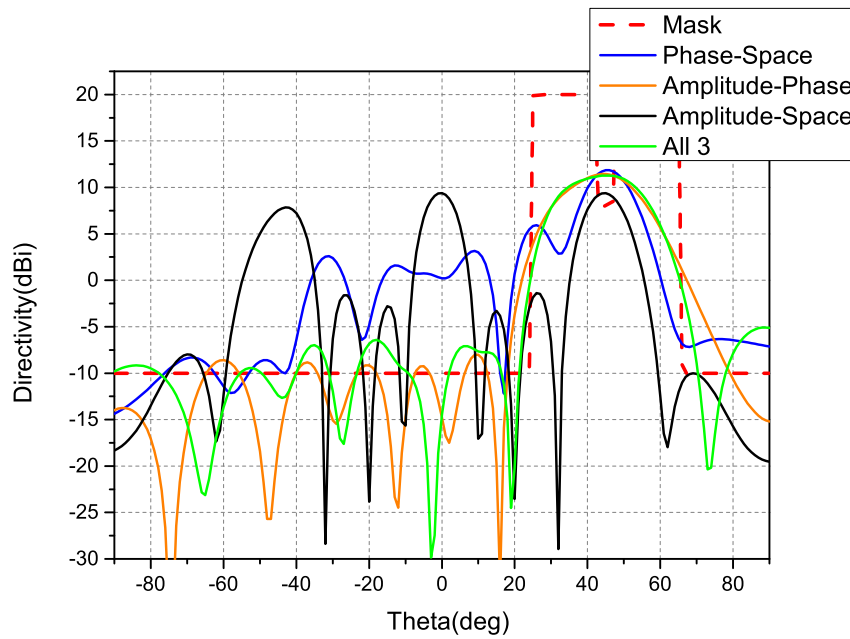


Fig. 9: Results with mask to steer the main lobe to  $45^\circ$  and to control the SLL using PSO.

influence of the directivity, since the contour of the pattern is more important than the directivity itself.

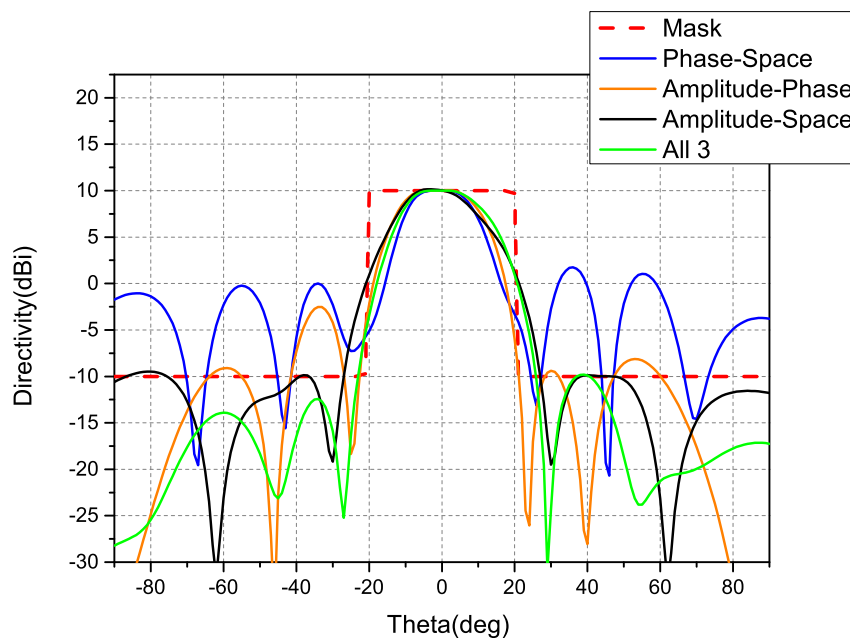


Fig. 10: Results with mask to flatten the main lobe from  $-10^\circ$  to  $10^\circ$  using PSO.

In general, PSO proves to be a powerful tool to optimize amplitudes, phases and spacings of an antenna array. A straightforward approach is to run PSO to optimize all three variables, but this increases complexity, hence making the solution much more



time consuming. However, according to the goal of the optimization, the choice of which parameters should be optimized can accelerate the process.

Because the optimization process is started with random numbers, PSO did not deliver the same set of coefficients every time it has been run, even though the mask has been fulfilled. Based on that, it is advisable to optimize more than once the same pattern. For the investigations presented above, PSO was run five times, but, in most cases, three optimizations are enough to produce reliable results. This effect is graphically shown and detailed in (SCHLOSSER et al., 2016) for the case of GA, but the same occurs with PSO.

### 3.2 NUMERICAL INVESTIGATIONS USING TAGUCHI'S METHOD

For all simulations, Taguchi's method was set with an orthogonal matrix with 81 rows and reduced rate of 0.9.

In Fig. 11, where the goal was to control the SLL and achieve a minimum level of directivity (at least 8 dBi), one can see that, in general, the results are slightly better than the ones obtained with PSO. When all three variables were optimized together, it is possible to see a significant difference between the results. Another observation is that there is not huge discrepancies in the directivity as observed in the results obtained with PSO. However, when phases and spacings are optimized, the worst result is obtained because of the same explanation pointed out previously.

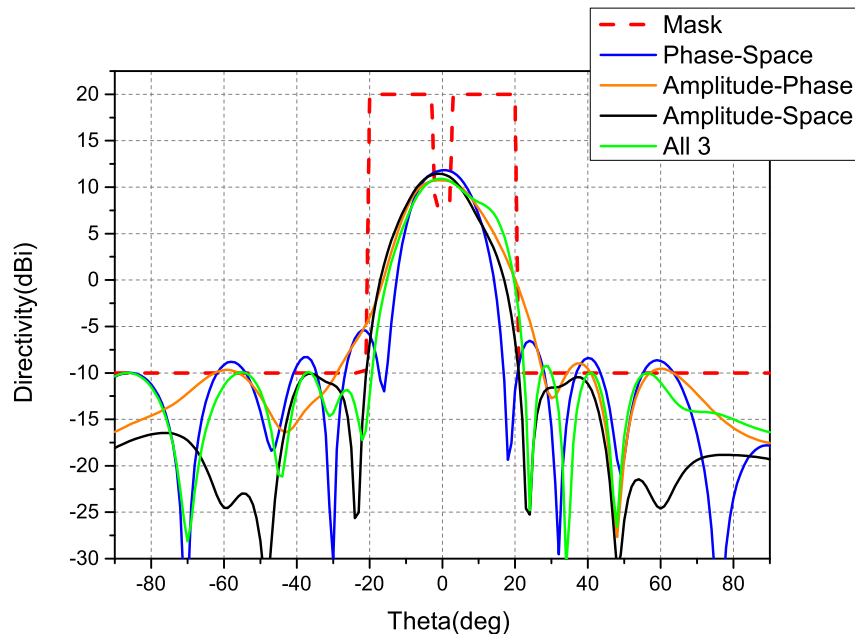


Fig. 11: Results with mask to control the SLL using Taguchi's Method.

Fig. 12, where the goals were the insertion of nulls in the pattern and SLL control, shows that the mask was best fulfilled when amplitudes and spacings and all three variables

were optimized. The conclusion is the same as for the results of PSO. However, in PSO, optimizing amplitudes and spacings provided higher directivity than the results with Taguchi's method.

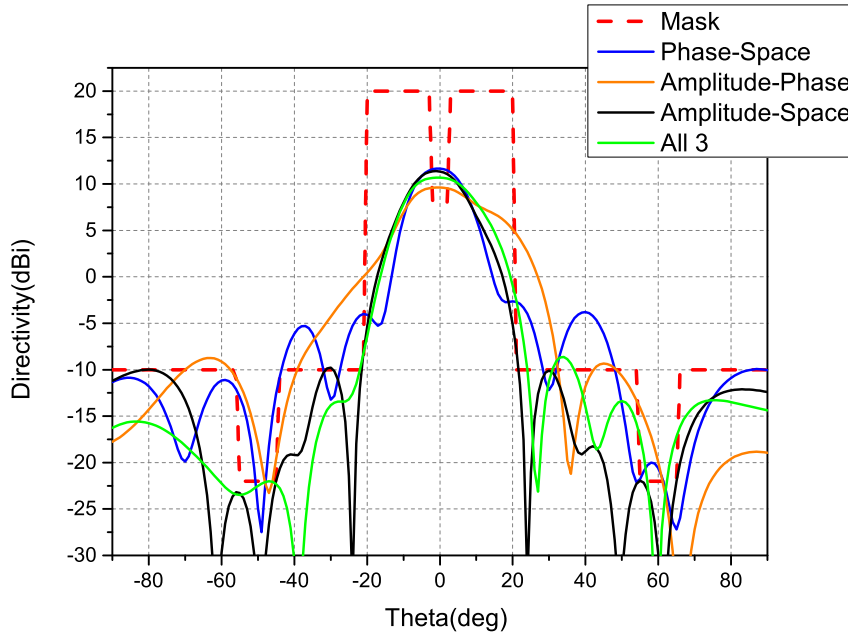


Fig. 12: Results with mask to control SLL and to insert nulls at  $-50^\circ$  and  $60^\circ$  using Taguchi's Method.

For the masks for steering the main lobe to  $30^\circ$  and  $45^\circ$ , shown in Figs. 13 and 14, respectively, in general, PSO achieved better results. The same conclusions extracted from PSO can also be applied here.

In the case of beamshaping shown in Fig. 15, PSO also achieved better results than with Taguchi's method.

### 3.3 COMPARISON OF TAGUCHI'S AND PSO ALGORITHMS

A fair comparison between both methods is difficult, because they are different in terms of principle of operation. While Taguchi's technique is deterministic, PSO is a stochastic heuristic. It is not possible to compare them in terms of number of iterations, because different number of experiments in each iteration is executed. On the other hand, a comparison in terms of time is not fair too, because Taguchi always starts with the same value for the variables while PSO is initialized with random numbers, hence the starting condition is different everytime PSO is run. By using a computer with the Intel Xeon CPU ES-2650 2.60 GHz and with 128 GB of RAM, both techniques took around 5 minutes for each optimization.

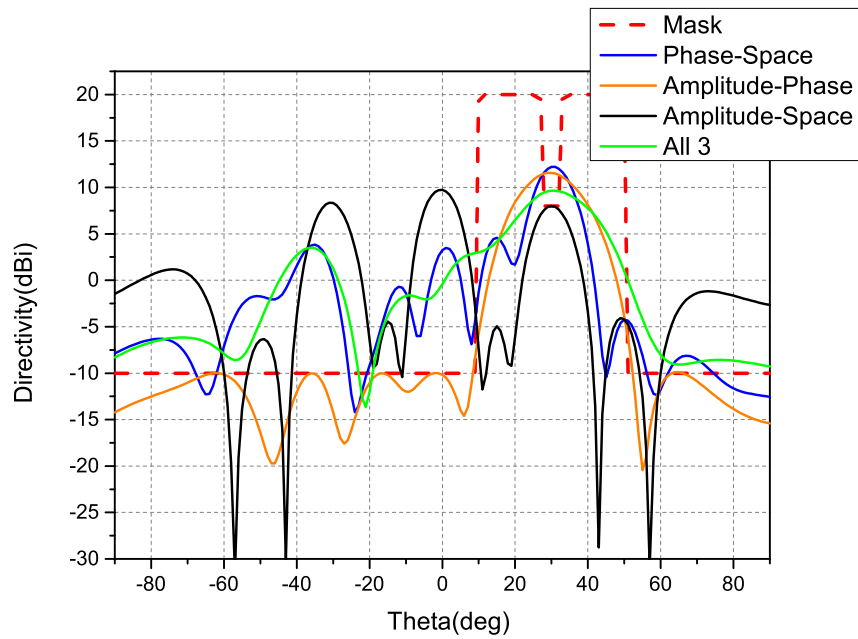


Fig. 13: Results with mask to steer the main lobe to  $30^\circ$  and to control the SLL using Taguchi's Method.

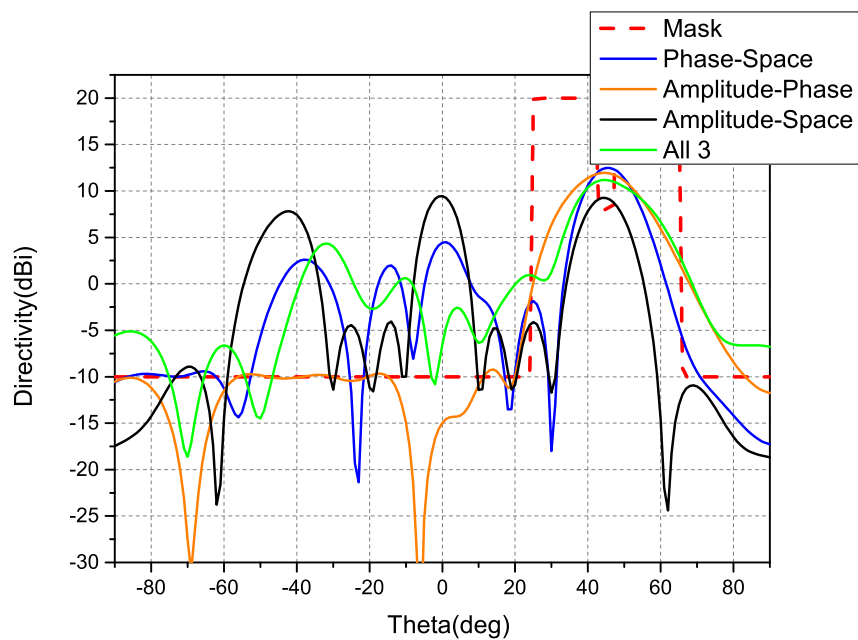


Fig. 14: Results with mask to steer the main lobe to  $45^\circ$  and to control the SLL using Taguchi's Method.

By considering these conditions, Taguchi's method is easier to be implemented and there is less parameters to set than PSO. Taguchi's method is also more reliable for embedded systems than PSO because it is deterministic (i.e. it always starts with the same values), hence providing always the same patterns. However, in the average, PSO

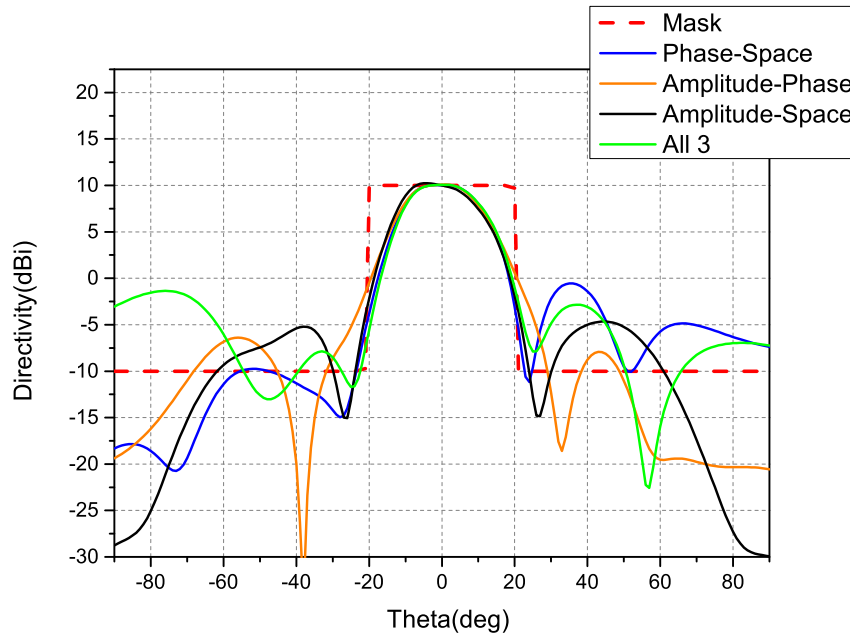


Fig. 15: Results with mask to flatten the main lobe from  $-10^\circ$  to  $10^\circ$  using Taguchi's Method.

produces better results in terms of fulfilling the masks than Taguchi's method and, by doing an investigation on its parameters and setting them accordingly, the best results will be surely achieved.

Thus, PSO proves to be better in the cases explored in this work. Because of that, for the following optimizations, only the PSO was used.

## 4 OPTIMIZATION OF A DUAL-BAND NON-UNIFORMLY SPACED ARRAY FOR MOBILE COMMUNICATIONS

The Brazilian mobile communication system has characteristics that were incorporated by the evolution of frequency allocation. One of them is the separation between operating frequencies for different applications such as 3G and GSM. For those, there are services allocated at 900, 1800, 1900 and 2100MHz.

This separation between the bands makes it necessary to use a wide-band antenna, which should operate from 824-2165 MHz, a dual-band antenna, which should be optimized for the bands 824-960 MHz and 1710-2165 MHz, or two single-band antennas. The problem with the first option is that this type of antenna is susceptible to interference. Besides that, it is hard to develop an antenna with band wide enough and stable radiation pattern over the whole band. Then, the second and the third options are the best based on this criteria. The drawback of the third option is that it requires more space in the towers, it is normally more expensive and requires more maintenance.

Thus, (FARIAS, 2014) proposed an antenna composed of two annular slots operating in two different frequencies. The author also presents a vast study of different types of antennas to cover the frequencies of the Brazilian mobile communication system. The antenna fulfills all requirements to operate in the Brazilian system such as operation bands from 0.824 GHz to 0.960 GHz and from 1.710 GHz to 2.165 GHz, high isolation between the ports and stable radiation pattern over the frequency in both bands.

Fig. 16 shows the geometry of the antenna (FARIAS et al., 2018). One can see that there are two concentric annular slots and, in the feeder line, there are matching and decoupling stubs in order to match the impedance and to keep both ports isolated. To achieve the desired gain and to shape the beam, this antenna has been used to compose an antenna array. The formats defined for the array pattern were ordinary main beam pointing to boresight and main beam with squared cosecant contour. The latter was chosen, because it allows illuminating a given area with the same power level in the cell that is covered by the array.

### 4.1 OPTIMIZATION FOR THE MAIN BEAM POINTING TO BORESIGHT

In order to avoid grating lobes, in most cases, the relative spacing between the elements in an array is set to be below  $\lambda_0$  (BALANIS, 2005). Due to the physical dimensions of the antenna proposed in (FARIAS, 2014), it is impossible to fulfill this condition, since, in the higher band, the resulting inter element spacing is equal to  $\lambda_0 = 158mm$  (at 1.9 GHz), so as to avoid overlapping. Because of that, grating lobes appear in the pattern of the higher band.

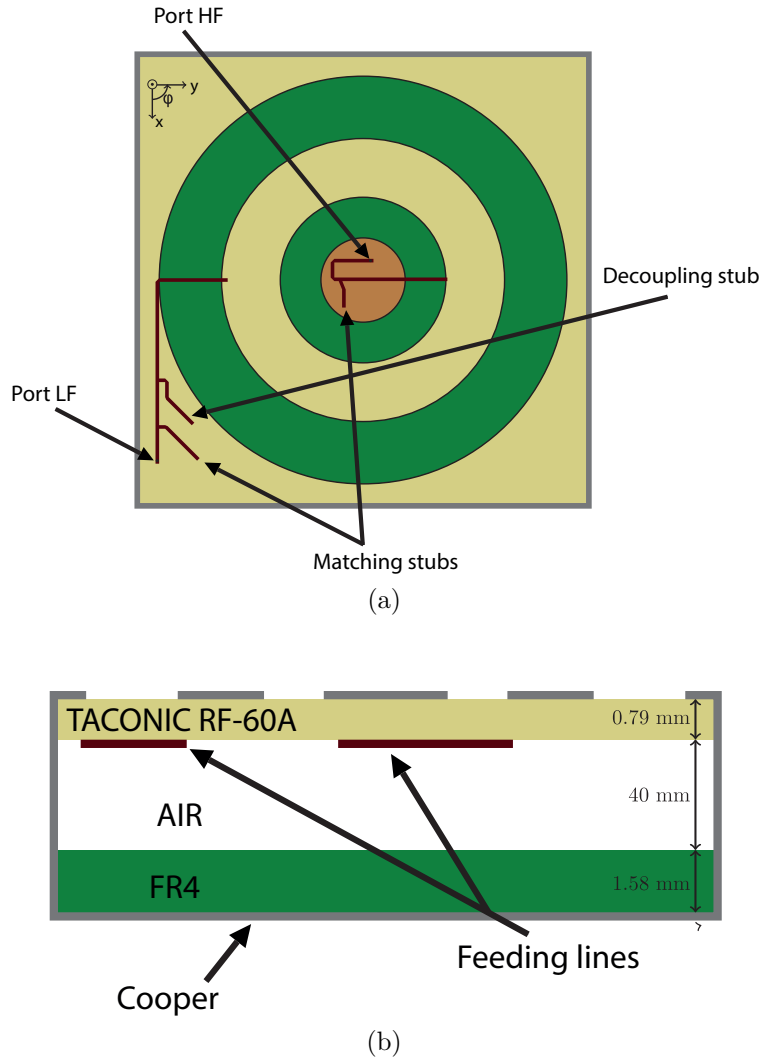


Fig. 16: Layout of the single element: (a) upper view and (b) front view (It was modified from (FARIAS, 2014)).

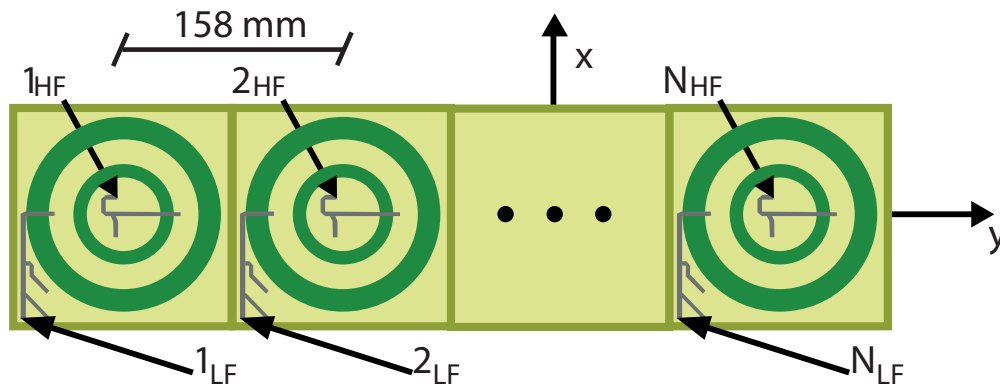


Fig. 17: Antenna array with annular elements (FARIAS, 2014)

The antenna array proposed by (FARIAS, 2014) is composed of seven elements and its geometry is shown in Fig 17. In order to suppress the grating lobes, the code developed in this work was used to find the optimum value of amplitudes, phases and

relative spacings between the elements. By optimizing just amplitudes and phases, as it is normally the case, good results could not be achieved. Then, it was necessary to include all the 3 parameters in the optimization. The resulting patterns for boresight radiation are shown in Fig. 18 (LEMES et al., 2017). The dashed red curve shows the mask, i.e the specifications the pattern must fulfill. The target is to keep the field intensity below the mask in all regions. The black curve (ULA) shows the pattern of the uniform linear array (amplitudes equal to 1, phases equal to  $0^\circ$  and relative spacings equal to  $\lambda_0$ ). The orange curve (S) shows the pattern found by optimizing just the relative spacings, the blue curve (A-S) just the amplitudes and spacings and, finally, the green curve (A-P-S) shows the resulting pattern when all the three parameters were optimized. This optimization was performed considering the single and isolated element.

Despite the blue and green curves were the best in terms of fulfilling the mask, the orange curve is considered to be the most interesting result, because the pattern level is above the mask only in small regions and the amplitudes and phases are the same for all elements. This means that the feeder has its complexity highly decreased. The balanced feeder is also good to avoid some undesirable effects such as unbalanced coupling between the feeder and the antennas, hence resulting less effort to design the antenna array.

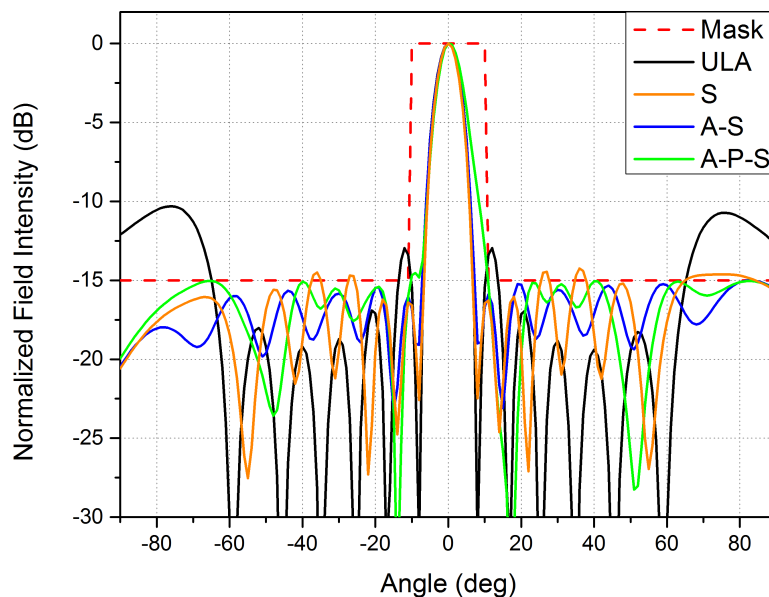


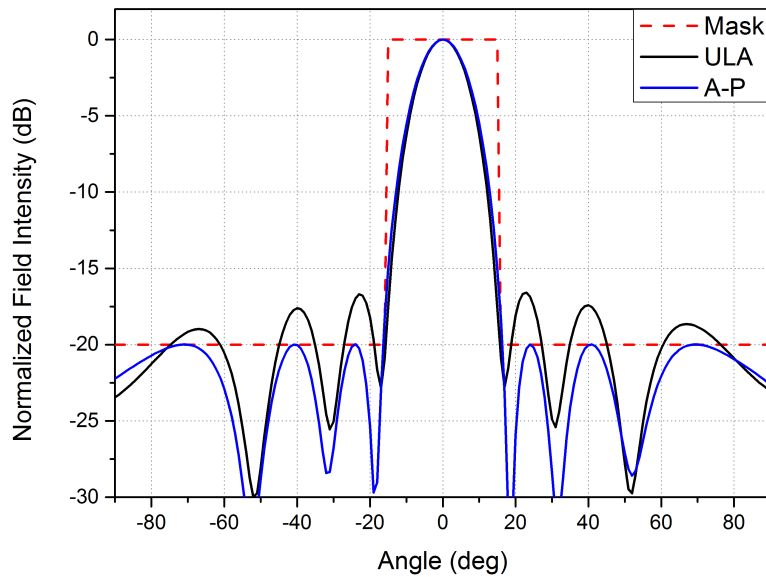
Fig. 18: Optimized patterns at 1.9 GHz with the main beam pointing to  $0^\circ$ .

Table 3 shows the inter-element spacings found by the optimization. One can see that only the last relative spacing is modified. According to (BALANIS, 2005), the grating lobes appear because of the periodicity existing in uniformly spaced array. By varying the position of element 7, this periodicity does not exist anymore.

|          | Inter-element spacing (mm) |
|----------|----------------------------|
| $d_{12}$ | 158                        |
| $d_{23}$ | 158                        |
| $d_{34}$ | 158                        |
| $d_{45}$ | 158                        |
| $d_{56}$ | 158                        |
| $d_{67}$ | 257.7                      |

Table 3: Inter-element spacings for the optimized dual-band antenna array.

Once the optimization for the higher band has been finished, the pattern for the lower band has been calculated. Since the elements are electrically closer to each other in this band, no grating lobes exist and the levels of the side lobes are also lower. The specification for the SLL is now 20 dB below the main beam. By taking the non-uniform positions optimized for the higher band and performing optimization of only the amplitudes and phases of the excitation coefficients, the optimized pattern for the lower band is shown in Fig.19. One can see that the patterns for both bands are pointing to the desired direction and with full control of the side lobe and grating lobe levels.

Fig. 19: Optimized patterns at 0.9 GHz with the main beam pointing to  $0^\circ$ .

A drawback of this optimization method is the fact that it is impractical to take mutual coupling (MC) into account for the optimization of the interelement spacings. The reason is that, during the optimization, many spacings are found and, for each one, a new full-wave simulation of the whole antenna array would be necessary. In order to estimate the influence of MC, two investigations are performed. The first (case 1) refers to the pattern shown in Fig.19, which means that the optimization was done using the pattern of



the isolated element without taking mutual coupling into account. In case 2, to account partially for the influence of MC, an antenna array with three elements equally spaced by  $\lambda_0$  was simulated and the pattern of the center element has been taken to perform the optimizations. By doing so, coupling to the neighboring elements was included for one fixed interelement spacing. This is still an approximation, since coupling with further elements was not taken into account. Moreover, this pattern is valid just for the element spacing equal to one wavelength.

The results were compared to simulations using the commercial software Ansys HFSS (ANSYS, 2016), which fully accounts for mutual coupling. Fig. 20 shows the results, where a good agreement has been obtained with the proposed optimization algorithm and the results simulated directly using HFSS. This validates the applicability of the proposed method. The accuracy of the optimization can be slightly improved when the approach including an approximation for the MC is used.

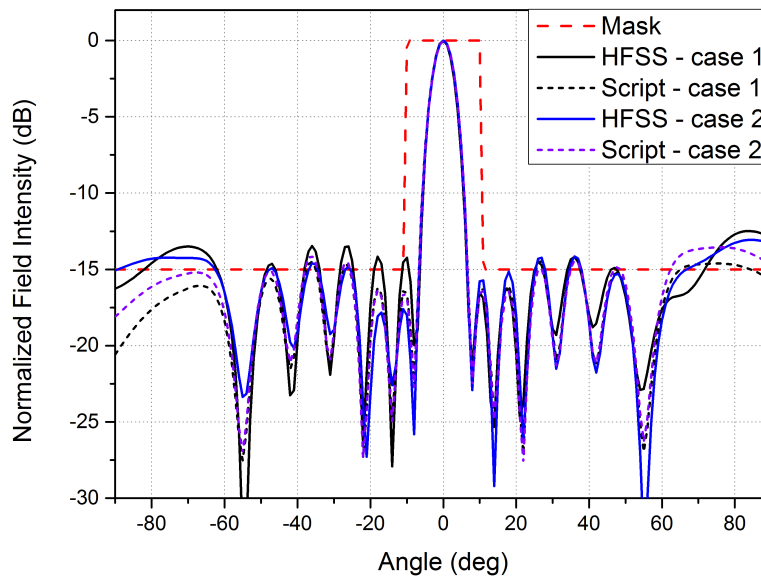


Fig. 20: Comparison using HFSS with amplitudes equal to 1 and all phases equal to 0.

## 4.2 OPTIMIZATION FOR THE MAIN BEAM WITH SQUARED COSECANT SHAPE

The next case deals with the main beam with squared cosecant shape and side lobe level control. In this case, the fitness function was set up as follows: on the shaped beam, the pattern should perfectly follow the contour (angular region between  $0^\circ$  and  $30^\circ$ ), whereas it should be below -15 dB in the other regions. Also in this case, the array design must be started with the higher band. As a first approach, the spacings optimized

in Fig. 18 have been considered here and only amplitude and phases have been optimized. This decision is justified due to the ability of the optimized spacings to mitigate grating lobes. The results are shown by the blue curve in Fig. 21. One can notice that one grating lobe still exists. In order to relax the specification of the squared cosecant contour, a tolerance of 2 dB has been allowed (black curve), and the grating lobe level is slightly decreased but does not disappear. Tolerances bigger than 2 dB are not allowed otherwise the pattern will not follow the cosecant contour. The resulting pattern for the lower band is shown in Fig. 22. In this case, all the specifications have been fulfilled.

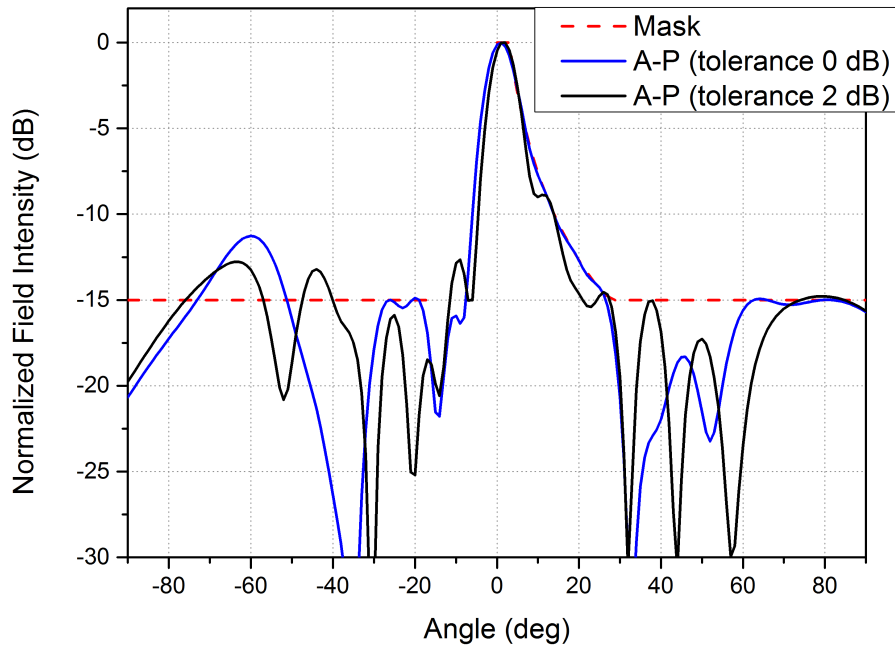


Fig. 21: Optimized patterns at 1.9 GHz with the main beam shaped as a squared cosecant.

Even without fulfilling all the optimization goals for the high frequency, due to the complexity of the mask and the high relative spacings between the elements, a validation using the commercial software HFSS (ANSYS, 2016) was performed. This validation was carried out in order to investigate the MC influence on the synthesis process into the pattern. Fig. 23 shows the patterns obtained using HFSS for the first case (without tolerance) in black and the second case (with tolerance equal to 2dB) in blue. The patterns do not deteriorate strongly. All beamforming coefficients are listed in tables 4 and 5

### 4.3 DESIGN PROCEDURE FOR ARRAYS COMPOSED OF DUAL-BAND DUAL-PORT ANTENNAS WITH WELL SEPARATED BANDS

In the previous sections, the investigations demonstrated that good performance in terms of low side lobe or grating lobe levels is hard to obtain for dual-band arrays

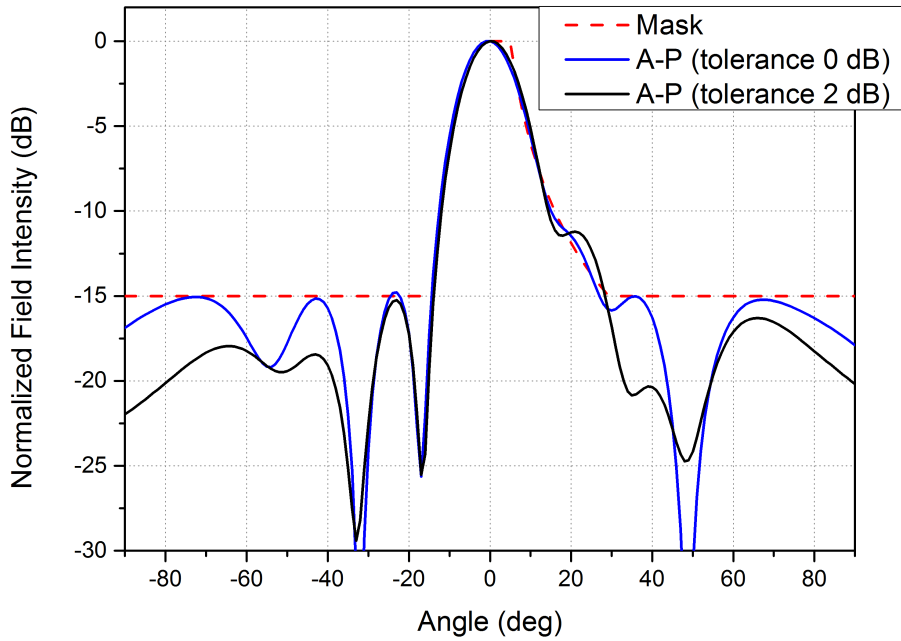


Fig. 22: Optimized patterns at 0.9 GHz with the main beam shaped as a squared cosecant.

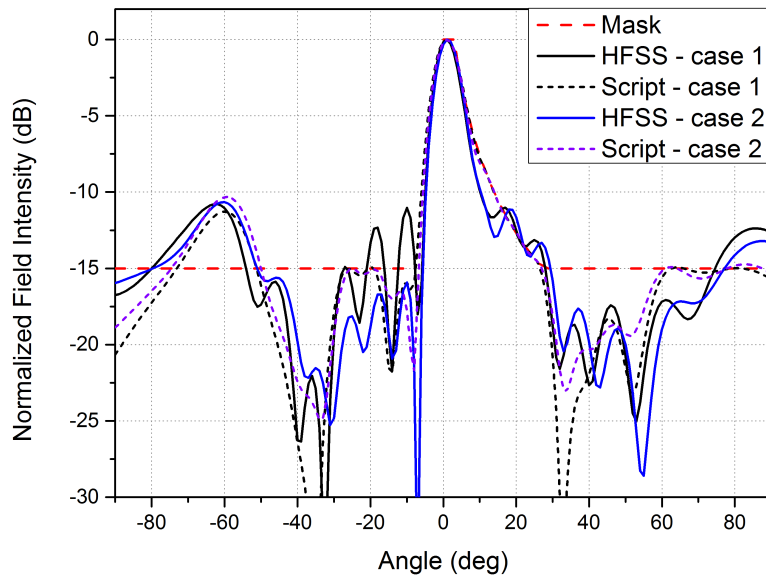


Fig. 23: Comparison using HFSS for the first case (without tolerance) and the second case (tolerance equal to 2dB).

whose bands are well separated. For this reason, a design procedure can be resumed in the following steps:

1. Optimization of amplitudes, phases and inter-element spacings for the higher band

| Port     | Normalized amplitude | Phase           | Port     | Normalized amplitude | Phase     |
|----------|----------------------|-----------------|----------|----------------------|-----------|
| $1_{LF}$ | 0.535                | $224.222^\circ$ | $1_{HF}$ | 1                    | $0^\circ$ |
| $2_{LF}$ | 0.782                | $230.863^\circ$ | $2_{HF}$ | 1                    | $0^\circ$ |
| $3_{LF}$ | 0.734                | $227.878^\circ$ | $3_{HF}$ | 1                    | $0^\circ$ |
| $4_{LF}$ | 0.981                | $229.834^\circ$ | $4_{HF}$ | 1                    | $0^\circ$ |
| $5_{LF}$ | 0.798                | $228.233^\circ$ | $5_{HF}$ | 1                    | $0^\circ$ |
| $6_{LF}$ | 1.000                | $229.915^\circ$ | $6_{HF}$ | 1                    | $0^\circ$ |
| $7_{LF}$ | 0.796                | $228.708^\circ$ | $7_{HF}$ | 1                    | $0^\circ$ |

Table 4: Excitation coefficients for radiation in the boresight with suppression of grating and side lobes.

| Port     | Normalized amplitude | Phase           | Port     | Normalized amplitude | Phase           |
|----------|----------------------|-----------------|----------|----------------------|-----------------|
| $1_{LF}$ | 0.254                | $186.066^\circ$ | $1_{HF}$ | 0.245                | $170.011^\circ$ |
| $2_{LF}$ | 0.306                | $221.763^\circ$ | $2_{HF}$ | 0.559                | $183.928^\circ$ |
| $3_{LF}$ | 0.362                | $243.678^\circ$ | $3_{HF}$ | 0.943                | $177.706^\circ$ |
| $4_{LF}$ | 0.527                | $223.296^\circ$ | $4_{HF}$ | 0.962                | $166.732^\circ$ |
| $5_{LF}$ | 0.356                | $236.800^\circ$ | $5_{HF}$ | 1.000                | $146.026^\circ$ |
| $6_{LF}$ | 0.951                | $238.085^\circ$ | $6_{HF}$ | 0.196                | $91.838^\circ$  |
| $7_{LF}$ | 1.000                | $219.669^\circ$ | $7_{HF}$ | 0.587                | $165.931^\circ$ |

Table 5: Excitation coefficients for the main beam with squared-cosecant shape.

in order to mitigate the grating lobes.

2. Simulation of the antenna array geometry in a full-wave electromagnetic simulator to extract the embedded patterns (also called active patterns) of the array elements, in order to take mutual coupling into account.
3. Run a second optimization, whereby only the amplitudes and phases are optimized for the higher band; at this point, the positions of the array elements are not changed anymore, so that the optimization is done including the effects introduced by mutual coupling on the radiation pattern of the whole array.
4. Optimization of amplitudes and phases for the lower band.

## 5 THE USE OF NON-UNIFORMLY SPACED ARRAYS FOR BEAMSHAPING WITH REDUCED NUMBER OF ELEMENTS

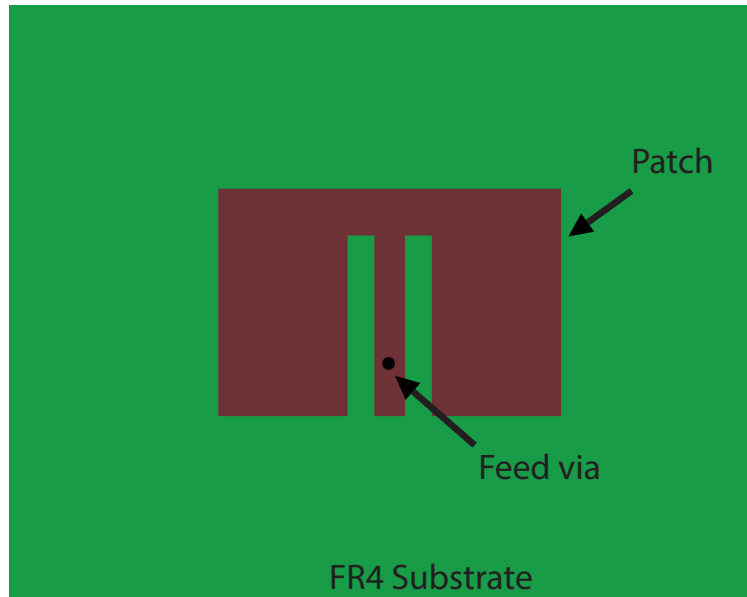
The proposed technique was applied to synthesize a pattern with squared cosecant shape as described in detail in (SCHLOSSER et al., 2016). The mask for the problem is described as follows: from  $-90^\circ$  to  $-6^\circ$ , which is the region of the side lobes, the goal is to keep the pattern below the mask; from  $8^\circ$  to  $90^\circ$ , the main beam must follow the squared cosecant contour. As shown in the previous chapters, this is required in order to illuminate a pico-cell with uniform power distribution. The authors of (SCHLOSSER et al., 2016) used seven E-shaped antennas uniformly spaced by half-wavelength from each other to reach the specifications, whereby the allowed deviation from the squared cosecant contour was 1 dB. Besides that, the authors also optimized the number of elements and, according to them, seven is the minimum number to reach the specifications. The single element that will be considered here is exactly the same as used by the authors, allowing a fair comparison between both designs. Fig. 24 shows the geometry of the single element developed in (SCHLOSSER et al., 2016).

### 5.1 APPLICATION OF THE PSO FOR THE PROPOSED PROBLEM

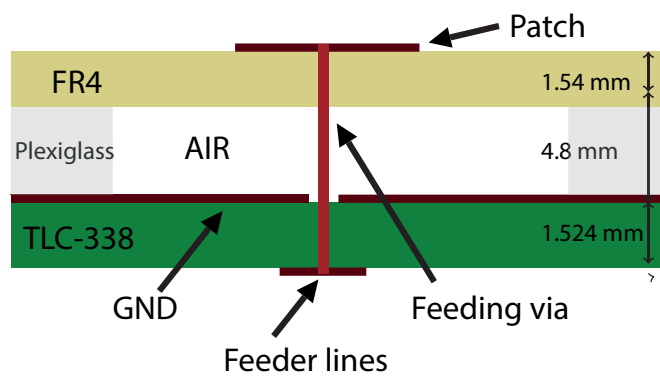
Despite the authors of (SCHLOSSER et al., 2016) successfully shaped the pattern with a cosecant contour, the complexity of the feeder was high and the size of the array was considerably large. Furthermore, the power level of some elements was quite low, which indicates that the use of non-uniformly spaced arrays could reduce the number of elements.

As the main goal was to decrease the number of elements whilst keeping the format of the pattern, a set of optimizations was done by varying the number of array elements. Fig. 25 shows the patterns of the non-uniformly spaced arrays, synthesized by the developed code, with different number of elements. One can see that the pattern of the array with 3 elements (blue curve) did not fulfill the mask (red dashed curve). The arrays with four (black curve), five (green curve) and six elements (purple) fulfilled the specifications. Therefore, the minimum array size that allows reaching the specified pattern is by using four elements, which means a reduction of 42.8% in the number of elements comparing to the use of an uniformly spaced array as described in (SCHLOSSER et al., 2016).

In order to optimize successfully non-uniformly spaced arrays, it is important to use a large number of particles and fine tune the social parameter. By doing so, the particles will be allowed to go over the whole search space more freely. Figs. 26 and 27 show the convergence of the  $g_{\text{best}}$  parameter in terms of amplitude and spacing values, respectively. The blue curves are the results obtained by setting  $c_1 = c_2$ , whereas the black curves are



(a)



(b)

Fig. 24: Layout of the single element: (a) upper view and (b) front view.

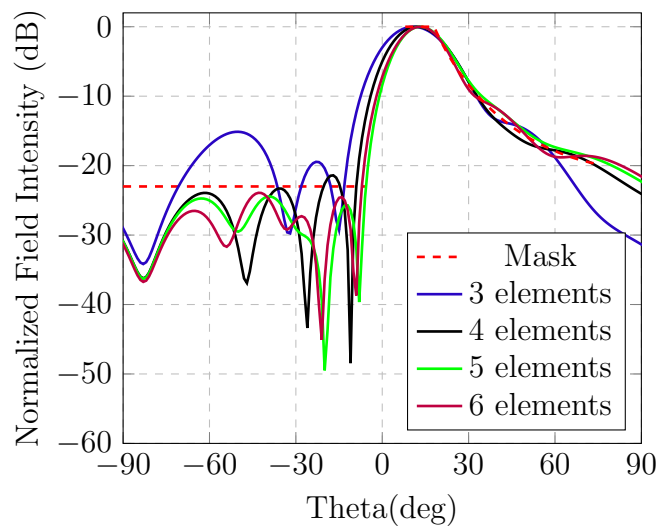


Fig. 25: Optimized patterns with different number of elements.

for  $c_1 = 1.5$  and  $c_2 = 0.3$ . For the present case, the oscillations always stop first in the black curve, hence proving that reducing the trust in the swarm improves the convergence for non-uniformly spaced arrays. The curves do not converge to the same value because there are more than one solution that fulfill the specified mask. The residual error is determined mainly due to small deviations of the synthesized pattern from the desired squared cosecant contour.

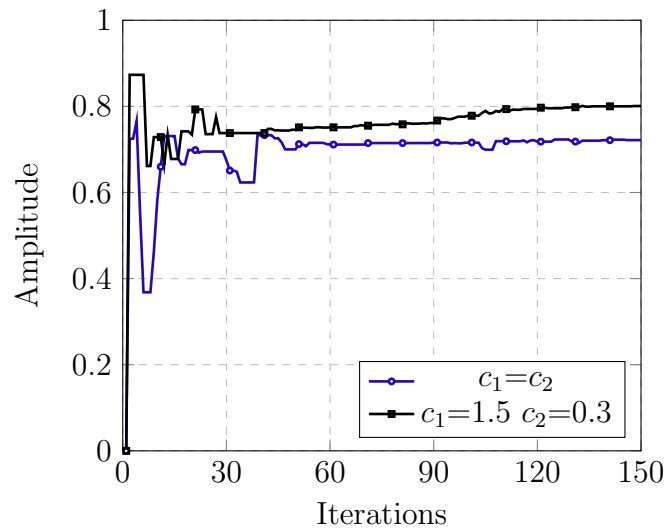


Fig. 26: Variation of the swarm's best position ( $g_{\text{best}}$ ) by optimization of the amplitudes after 150 iterations.

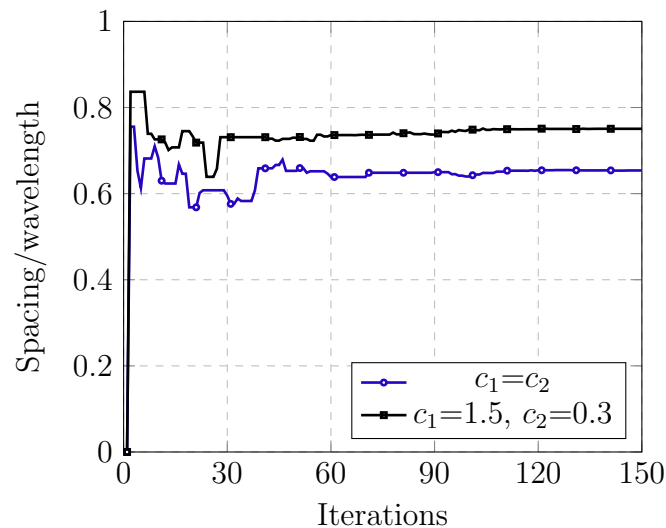


Fig. 27: Variation of the swarm's best position ( $g_{\text{best}}$ ) by optimization of the spacings between the elements after 150 iterations.

The influence of varying the  $c_1$  and  $c_2$  parameters can be visualized Fig. 28. The PSO converged to a smaller residual error by applying different values for  $c_1$  and  $c_2$ . The initial values for both curves are not the same, because the PSO has been started with random values for amplitudes, phases and spacings. Although the starting points for both

cases are different, there is no great impact in the final convergence, since the fitness function decays rapidly in the first few iterations.

The effect of the residual error in the synthesized pattern can be observed in Fig. 29. It is clear that the differences are more remarkable especially for theta values larger than  $50^\circ$ .

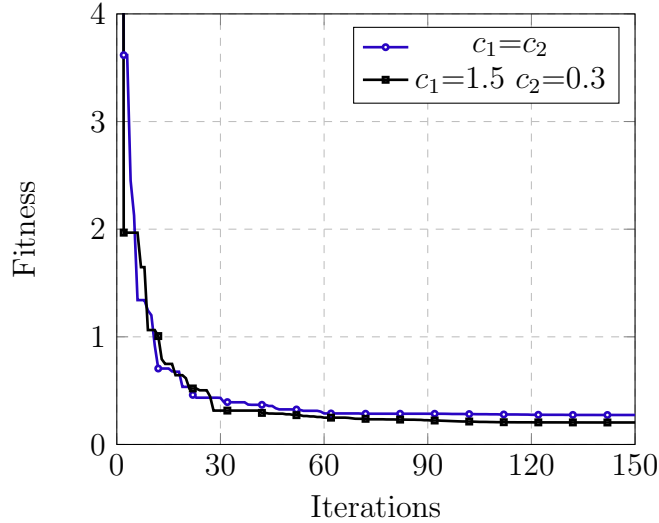


Fig. 28: Variation of the fitness function (error) using different values for the self-confidence ( $c_1$ ) and the trust in the swarm ( $c_2$ ).

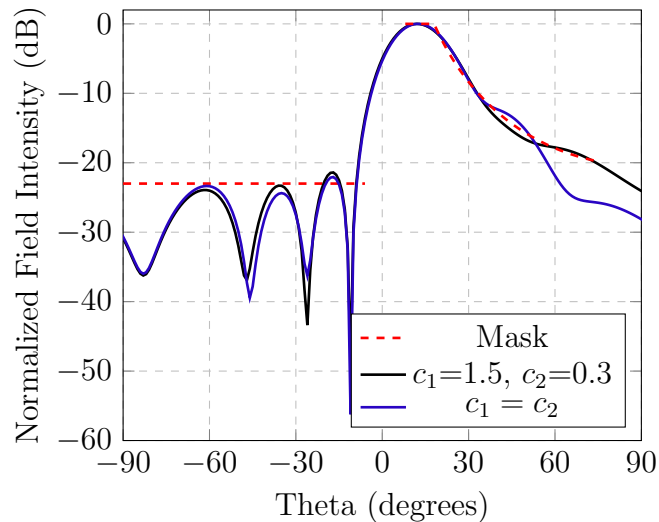


Fig. 29: Synthesized patterns using different values for the self-confidence ( $c_1$ ) and the trust in the swarm ( $c_2$ ).

Table 6 shows the relative spacings between the antennas found by the first round of optimizations.

Fig. 30 shows the comparison between the pattern synthesized and the pattern calculated with HFSS (ANSYS, 2016). The discrepancy between them is due to the mutual



Table 6: Center-to-center spacings found by the first optimization

|          | Spacings (mm) |
|----------|---------------|
| $d_{12}$ | 105.2         |
| $d_{23}$ | 71.5          |
| $d_{34}$ | 85.5          |

coupling. In order to compensate the MC, another optimization was performed. With the spacings found previously, the pattern of each element was exported from HFSS, which means that the MC was now taken into account. A new run of PSO was carried out, whereby only the amplitude and phase for each element have been optimized again. The result is shown in Fig. 31, where the result synthesized by (SCHLOSSER et al., 2013) is also plotted. One can see that the mask has been fulfilled taking into account the allowed deviation.

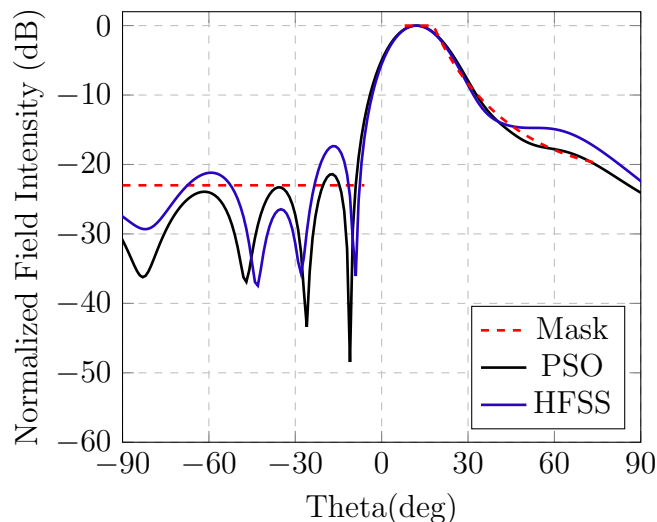


Fig. 30: Comparison between the pattern synthesized with the proposed technique (black curve) and the pattern calculated with HFSS (ANSYS, 2016) (blue curve). The red curve is the mask considered for the optimization.

## 5.2 FEEDER DESIGN

Table 7 shows the normalized amplitude and phase for each antenna after the second optimization. One can see that the power that should be delivered to antenna 3 is 8.1 times larger than to antenna 1 and 3.56 times larger than to antenna 4. Such power division ratios are hard to produce using passive splitters because the transitions between the line widths are too big. On the other hand, the huge phase shift along with the different spacings between the elements provide differences in the total length between the port and each antenna, which yields a narrow band behavior. By analyzing this trade off, it was decided to group the antennas with similar power level. With this approach,

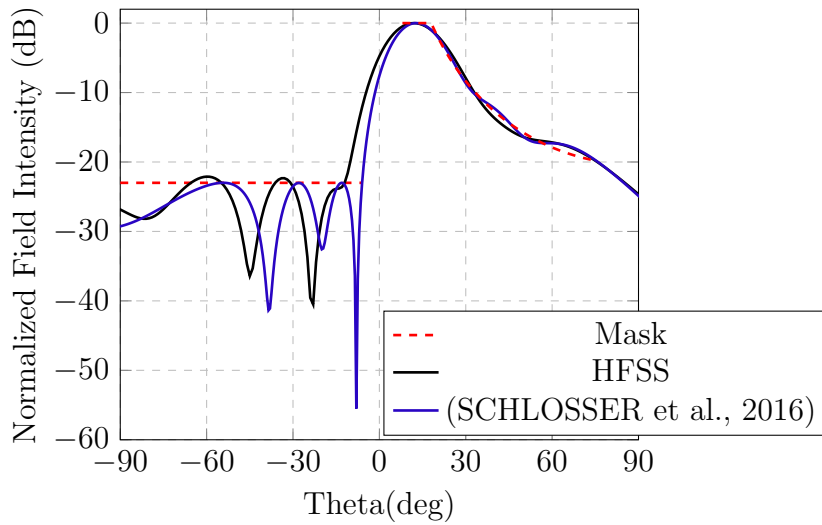


Fig. 31: The final pattern obtained with the second optimization (with 4 elements) and the pattern obtained by (SCHLOSSER et al., 2016) (with 7 elements).

Table 7: Normalized Amplitude and Phases of each antenna found after the second optimization

| Antenna | Normalized Amplitude | Phase (deg) |
|---------|----------------------|-------------|
| 1       | 0.1234               | 264.65      |
| 2       | 0.6682               | 218.95      |
| 3       | 1                    | 155.55      |
| 4       | 0.2806               | 95.06       |

it was possible to avoid lines with width smaller than 1 mm, which would be critical to implement due to the tolerance of the manufacturing process, and lines with width larger than 6 mm, to minimize spurious radiation from the feed network.

Antennas 1 and 4 were grouped by the power divider shown in red in Fig. 32. The input of this divider was connected to antenna 2 by the power divider shown in pink. Finally, the splitter marked in white is responsible for the correct power division between antenna 3 and the remaining antennas in the array. The drawback of this approach is the coupling between the splitters during the development of the feeder. An iterative process was required in order to compensate the coupling between them. By doing this, the splitter in red has the division ratio of 1:2.27, the splitter marked in pink has 1:1.65 and the splitter in white 1:1.07, hence proving that the chosen layout mitigated the problem with the power division ratios.

After defining how the antennas were grouped, the input impedance of each antenna, including mutual coupling, must be known. In order to obtain the input impedance, a line section of  $50 \Omega$  with length of  $\lambda/8$  was added after each via. These lines are highlighted in yellow in Fig. 32 and their purpose is to allow mitigating the effect of the transition between the via probe and the line. The line length was chosen after proving, by simulation

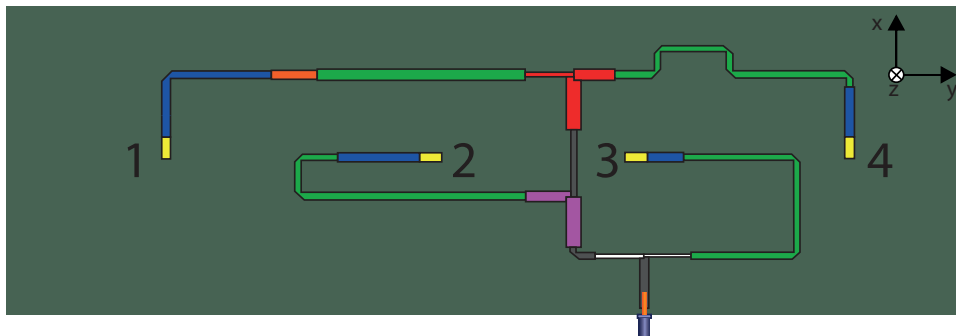


Fig. 32: The design of the proposed feeder split in parts.

Table 8: Input impedances of each antenna taking into account the mutual coupling.

| Antenna | Impedance   |
|---------|-------------|
| 1       | 48.1-j18.63 |
| 2       | 59.57-j5.79 |
| 3       | 41.27+j6.87 |
| 4       | 43.75-j1.28 |

using HFSS, that the field is already stabilized. Then, the input impedances were obtained and are shown in Table 8.

After obtaining the input impedance of each antenna, additional  $50 \Omega$  line sections were added in order to compensate the reactance of each antenna. The input impedances were moved to the real axis of the Smith chart. Those lines are highlighted in blue in Fig. 32. A particularity occurs in antenna 1 because the resistance found was too large, providing a line with width smaller than 1 mm. Because of that, a quarter-wavelength transformer was added and then the resistance transformed to  $50 \Omega$ . Table 9 shows the length of the lines and the respective resistance after the lines.

Table 9: Input impedances of each antenna taking into account the mutual coupling.

| Antenna | Length (mm) | Resistance ( $\Omega$ ) |
|---------|-------------|-------------------------|
| 1       | 26          | 78.22                   |
| 2       | 31          | 62.30                   |
| 3       | 14          | 69.23                   |
| 4       | 19          | 63.67                   |

Then, a line sections enough to interconnect the splitters (marked in gray in Fig. 32) and the antennas, and also to produce the desired relative phase shifts were added. Such line widths are calculated according to each resistance found previously and are marked in green in Fig. 32.

Fig 33 shows the pattern prior to the integration of the feeder (black curve), the simulated patterns with the coefficients found by PSO (blue curve) and the pattern obtained by simulation with the complete system integrated (green curve). The small

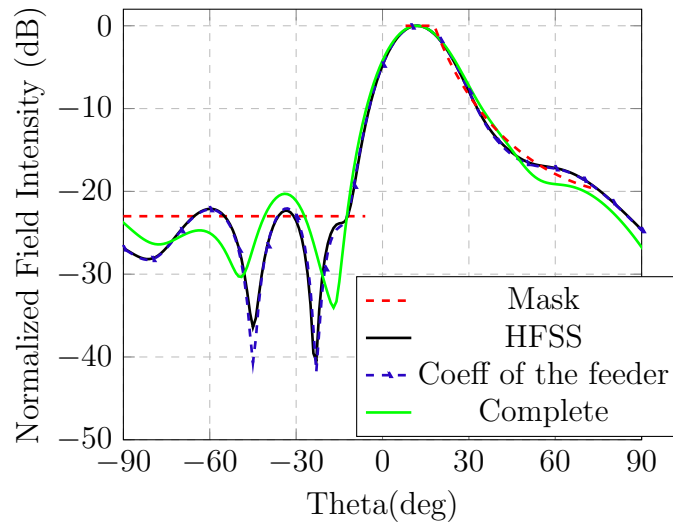


Fig. 33: The pattern obtained with the coefficients of PSO, the pattern obtained with the coefficients delivery by the developed feeder and the pattern of the integrated system, all of them calculated with HFSS (ANSYS, 2016).

differences between the complete system and the other curves are due to coupling effects between the antennas and the feeder and the spurious radiation. Despite there is a ground plane between them, some coupling still exists. Comparing the curves blue and black, it is clear that the coefficients of the developed feeder are satisfactory to generate the desired pattern since the curves almost overlap in the region of the main lobe.

### 5.2.1 FABRICATION OF THE DESIGNED ARRAY

Before starting the fabricating process, validation of the permittivity of the substrate has been done. The substrate chosen for the feeder was the Taconic TLC 338 (TACONIC, ), the same used in (SCHLOSSER et al., 2013). The validation was done by building up a splitter and doing a parametric study with HFSS (ANSYS, 2016). Fig. 34 shows a picture of the developed splitter. In the datasheet of the used substrate, the manufacturer states that the relative permittivity of the TLC-338 is 3.38. However, by analyzing the parametric study and the measured curves in Fig. 35, one can see that the real relative permittivity is 3.23. Because of that, the feeder was developed by setting  $\epsilon_r = 3.23$  in HFSS.

After the development of the feeder and the validation of the permittivity, a prototype was fabricated, built up and is shown in Fig. 36. Due to the manufacturing constraints of the milling machine, one can see in Fig. 36 a that the upper layer was split into two parts. Despite those limitations, the prototype was assembled and the measured results will be shown in the next section.

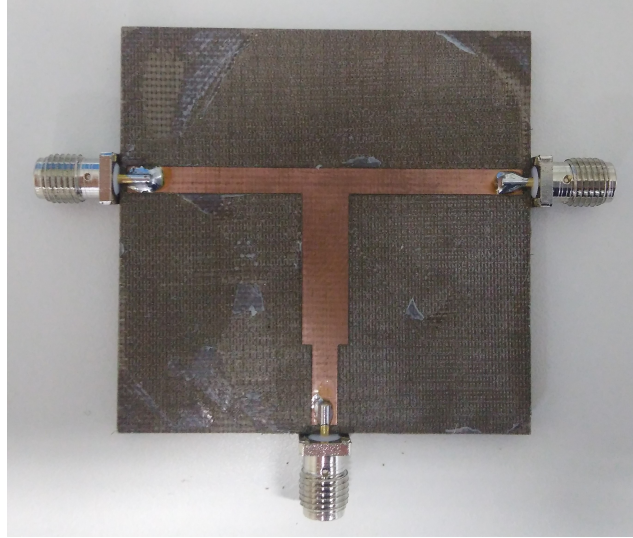


Fig. 34: Upper view of the fabricated splitter.

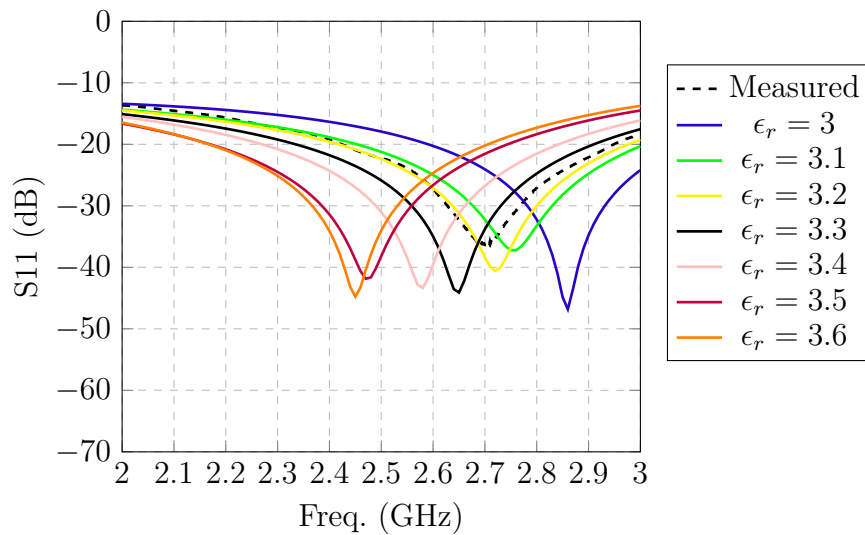


Fig. 35: Measured and simulated parametric curves of the developed splitter.

### 5.2.2 EXPERIMENTAL VALIDATION OF THE DESIGNED ARRAY

Fig. 37 shows the setup used for the measurements. The minimum distance of the far field was calculated and the antennas were positioned according to this distance as shown in Fig. 38.

Fig 40 shows a comparison between the simulated pattern including the feeder (black curve), the measured pattern (blue curve) and the measured pattern obtained by (SCHLOSSER et al., 2013) (green curve). Some discrepancies were found comparing the simulated and measured patterns and are mainly due the fabrication tolerances and ground reflexions during the measurements. Nevertheless, the measured results indicate the possibility of beamshaping with simultaneous sidelobe level control.

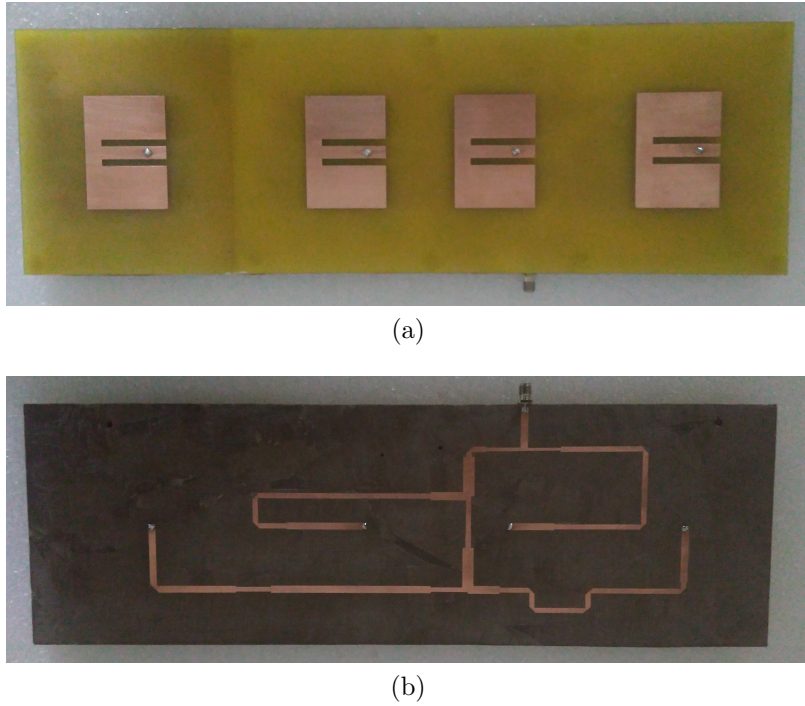


Fig. 36: Prototype of the proposed antenna array: (a) upper view and (b) bottom view.

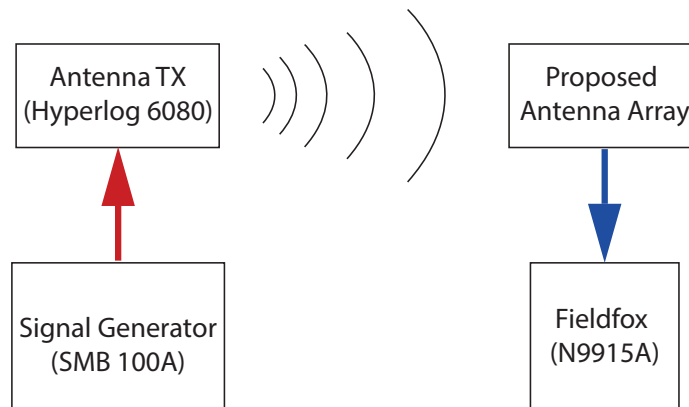


Fig. 37: Setup of measurements.

In Fig. 39, it is shown the measured result of the  $S_{11}$  parameter and one can see that the feeder operates satisfactorily in the whole band, which means  $S_{11}$  below  $-15$  dB. This limit was chosen as one of the guidelines of the whole project.

The measurements proved that the non-uniformly array provided such as good results as the ones reported in (SCHLOSSER et al., 2016).

### 5.3 PROCEDURE FOR THE DESIGN OF NON-UNIFORMLY SPACED ARRAYS

After the successfully design described in the previous sections, the following guidelines can be summarized:



Fig. 38: Picture of the setup. Highlighted on the right it is the Tx antenna and on the left the proposed antenna array.

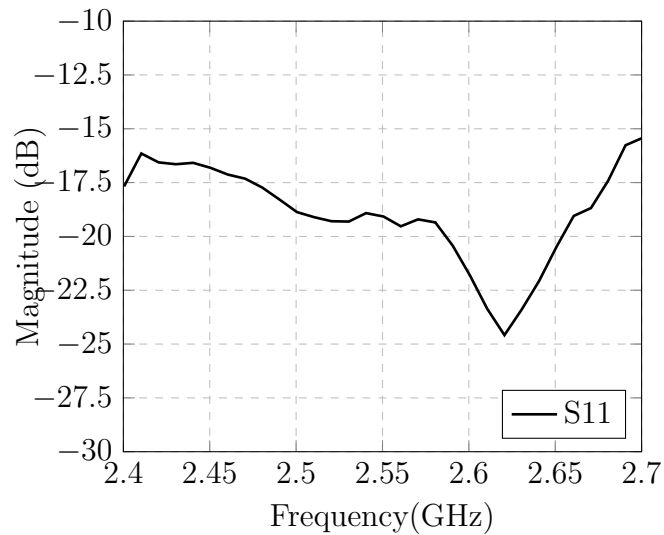


Fig. 39: Measured result of the S11 parameter.

1. The design may start with the determination of the minimum number of elements needed to achieve a given mask by employing non-uniformly spaced arrays.
2. Once the minimum number is found, the pattern of a single and isolated element, which is intended to be used to compose the array, should be used to optimize the inter-element spacings.
3. The third step is the electromagnetic modeling of the non-uniformly spaced array in a full-wave simulator, so as to extract the embedded patterns of each array element including mutual coupling effects.
4. The embedded patterns can be imported in the optimization tool, which should be used for the second round of optimization of amplitudes and phases of the excitation



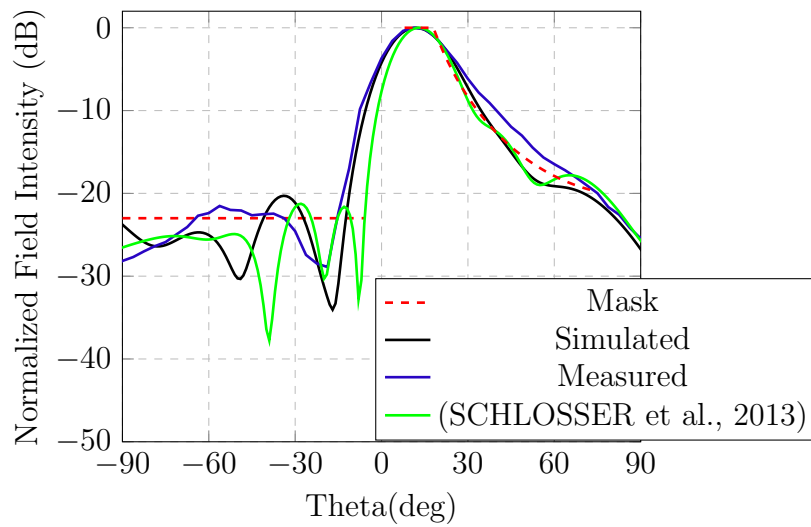


Fig. 40: The simulated pattern, measured pattern and pattern by (SCHLOSSER et al., 2013).

coefficients (at this point, spacings are not changed anymore).

5. Finally, the feeder can be designed and the array manufactured.



## 6 DEVELOPMENT OF TRANSMITTER CIRCUITRY FOR ADAPTIVE BEAM-FORMING

After calculating the best set of coefficients using the code proposed previously, the power levels and phases calculated need to be delivered to each antenna of the array. There are two ways to achieve it. The first one is using passive structures such as the feeder developed in section 5. The second one is using active components. Although it is more complex in most cases, the latter allows changing the coefficients, which means that the pattern of the array can be modified.

In this chapter, a modular adaptive transmitter that allows performing analog and digital beamforming by using digitally controlled variable gain amplifiers (VGA) and phase shifters (PS) is presented. The modular approach allows using the device for different transmit frequencies and thus makes the design very flexible. Distinctive features are low cost and power consumption as well as good reproducibility of performance.

The main priority of the project is the cost, so the decisions were made mainly based on this principle: minimization of costs. Along the project, the goals were reviewed and this evolution will be shown in the next section, where a chronological view of the design will be presented.

The transmitter developed has the capability to control the power level and the phases of the signal. Besides that, high gain and frequency translation capability were required. The signal is generated by the Field-Programmable Gate Array (FPGA) and has to be mixed up from 500 MHz to 7 GHz in order to be transmitted by the antenna array.

### 6.1 OVERVIEW OF THE DESIGN

The old version of the transmitter was developed by (MAGALHAES, 2017) and is shown in Fig 41. This layout does not include variable gain amplifier (VGA), i.e. it is impossible to control the power level to compensate the intrinsic unbalance between the front-ends (calibration) and to shape the beam. Besides that, the gain is slightly above 0 dB, which is not acceptable in this work. Another drawback of this layout is the size: because of the low-pass filter, the size of the printed circuit board (PCB) is large, hence yielding higher fabrication costs. The design also does not include phase shifters. In order to utilize the components already available, it was decided to design and to fabricate a new version replacing the filters by commercial parts and, in order to measure the behavior of each component, some fixed-pitch compliant (FPC) footprints were included, which allow the use of the probe station for S-parameter measurements. The first version of the transmitter design in this work is shown in Fig 42.

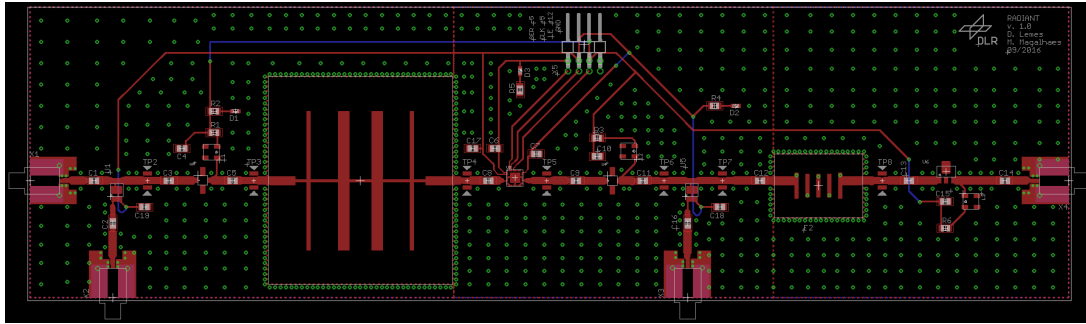


Fig. 41: Old Version downscaled designed by (MAGALHAES, 2017)

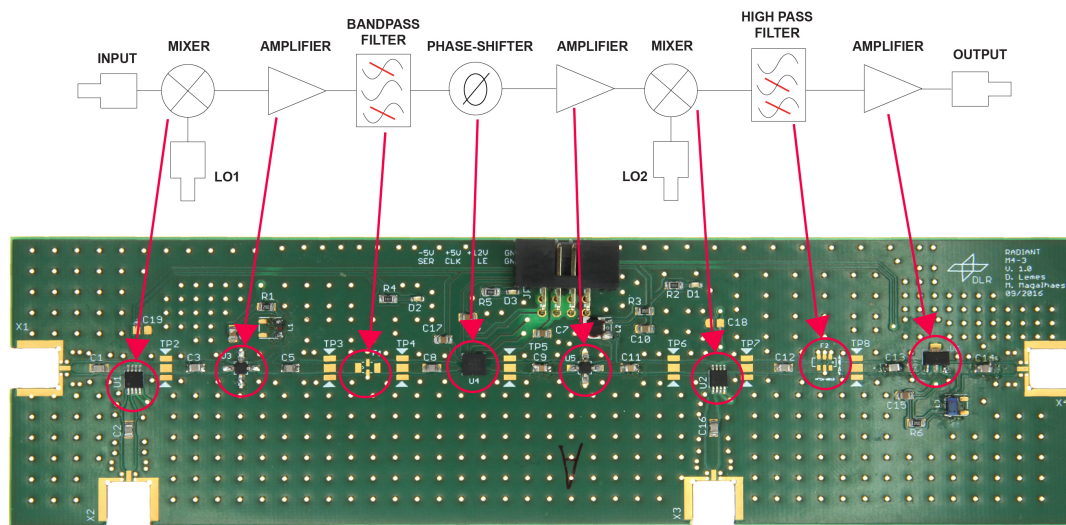


Fig. 42: First layout designed in this work.

The first layout allowed obtaining the S-parameters of most of the components. The amplifiers in 1.9 GHz did not exhibit the expected gain. Because of that, many investigations were done. A schematic of the amplifiers is shown in Fig. 43. Measured curves are shown in Fig. 44, where it becomes clear that the choke TCCH-80+ was not a good choice because its self resonance frequency is near to the frequency of work. Since the system will be used in 1.9 GHz, all other combinations between the inductor and capacitor provided good results. A capacitor with 1 nF and the inductor with 560 nH were chosen. As expected, Fig. 44 shows that the smaller the component, the higher is its self resonance frequency.

In the second version, shown in Fig. 45, the capacitors and inductors were changed and the FPC-footprints were removed. During the measurements, the gain level was still not as expected and also ripple was present. After that, by using a semi-rigid cable, all components were measured separately. The conclusions were that the gain level problem came from the last amplifier, which operates at 7GHz and the ripple came from the second mixer stage, which translates the signal from 1.9 GHz to 7.0 GHz.

Experiments with different capacitor sizes and capacitances were done, in order to

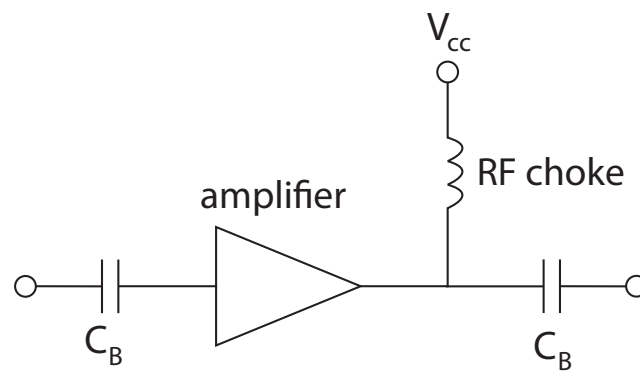


Fig. 43: The schematic of the amplifiers at 1.9 GHz.

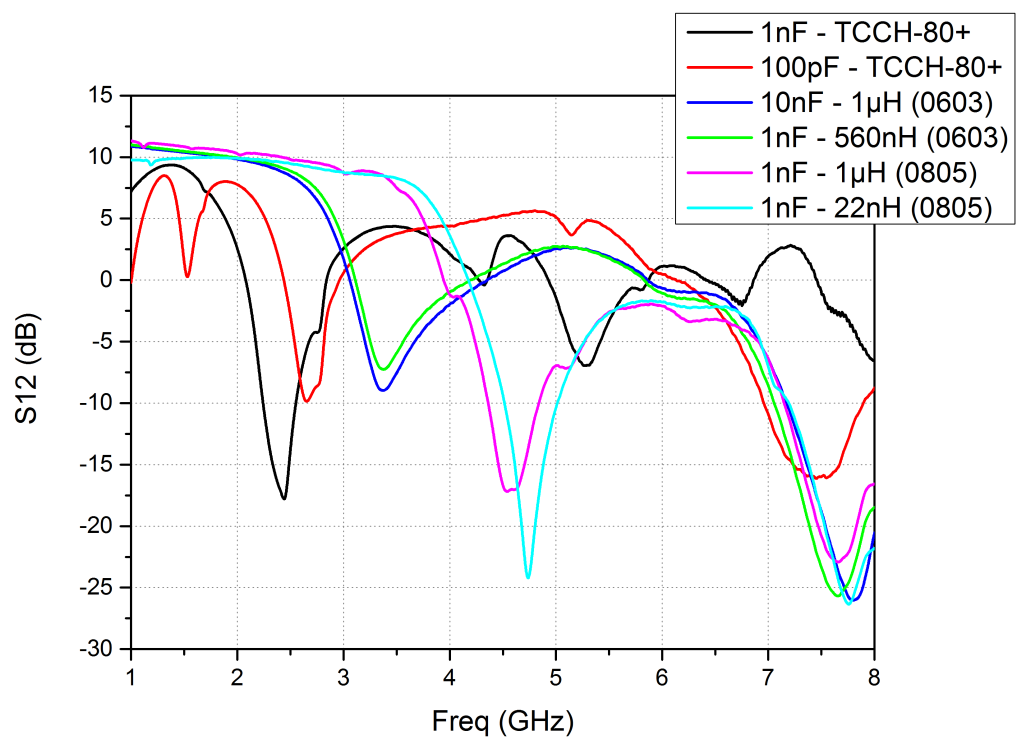


Fig. 44: S-parameters for different sets of capacitors and inductors.

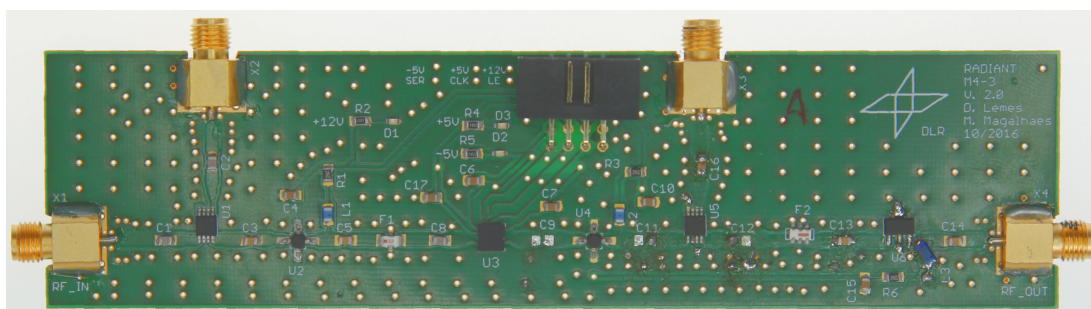


Fig. 45: Second layout designed in this work. Without FPC and mixers place correctly.

mitigate the ripple problem but none of them yielded good results. In 7 GHz, the changes are more sensible and, based on that, the inductor (L3) was soldered directly on the 50  $\Omega$  line which achieved better results. The datasheet advises the insertion of vias on the ground pins of the amplifier. By doing this manually, the measured gain curve was as expected, which means an increase of around 4 dB related to the previous version. These modifications are highlighted in Fig. 46.

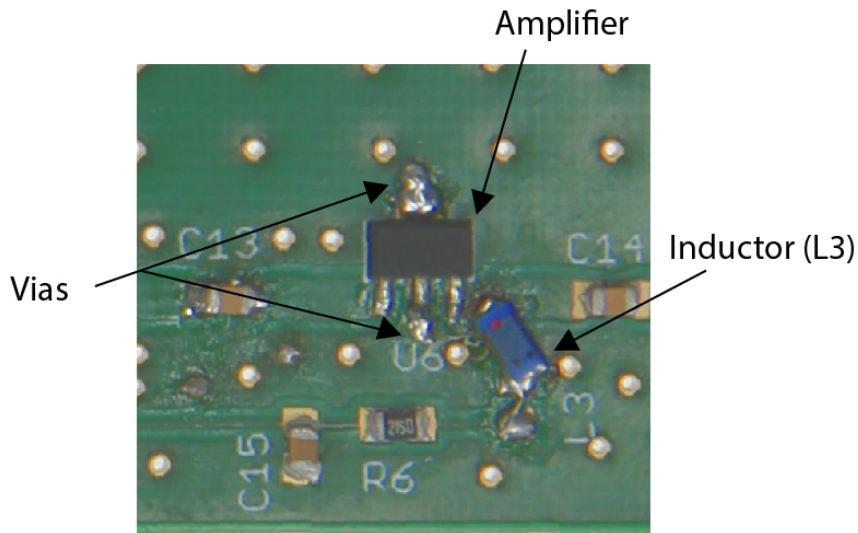


Fig. 46: Insertion of vias and inductor (L3) soldered directly on the 50  $\Omega$  line

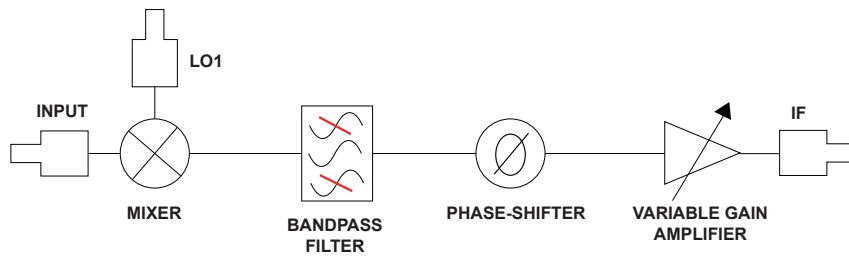
In the final design, shown in the next section, these modifications were implemented, all amplifiers but the last one, in 7 GHz, were replaced by a VGA and also the second mixer stage was replaced.

## 6.2 FINAL DESIGN

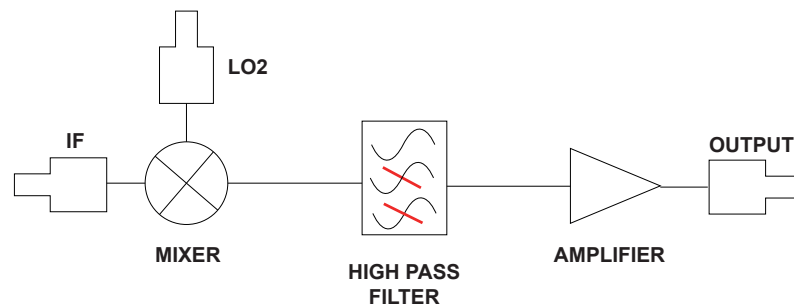
The transmitter was split into two parts: the beamforming and the upconverter modules, whereby both should be connected in series. The block diagrams of both units are shown in Fig. 47. The beamforming unit takes a baseband or low frequency input and mixes it up to an intermediate frequency as shown in Fig. 47a. A bandpass filter limits the signal to the frequency range at which the subsequent phase shifter works with nominal performance. This PS and also the subsequent VGA are digitally controlled and used to adjust amplitude and phase of the input signal.

As the operation frequency of phase shifters is usually limited, to achieve the desired transmit frequency, the upconverter module in Fig. 47b was designed. This circuit consists of another mixer stage, a highpass filter, and a RF amplifier. The choice of components and local oscillator (LO) signal defines the transmit frequency of the whole transmitter.

The proposed design concept offers distinct advantages. Through the use of two separate modules, the frequency plan is very flexible. The beamforming module is quite



(a)



(b)

Fig. 47: Block diagrams of the two transmitter modules: (a) Beamforming unit composed of a mixer, a bandpass filter, a phase shifter and a VGA; (b) Upconverter stage composed of mixer, highpass filter and amplifier.

generic and can be used in combination with different upconverter modules. The upconverter, on the other hand, can be designed to suit the desired transmit frequency and necessary output power. Additionally, having the steerable components on the IF makes the printed circuit board (PCB) design easier. The lower frequencies are less susceptible to impedance mismatch and ground plane interruptions. These occur due to the necessary control lines that have to be implemented. When designing the upconverter module, one can focus on good RF design practice.

### 6.3 FABRICATED PROTOTYPES

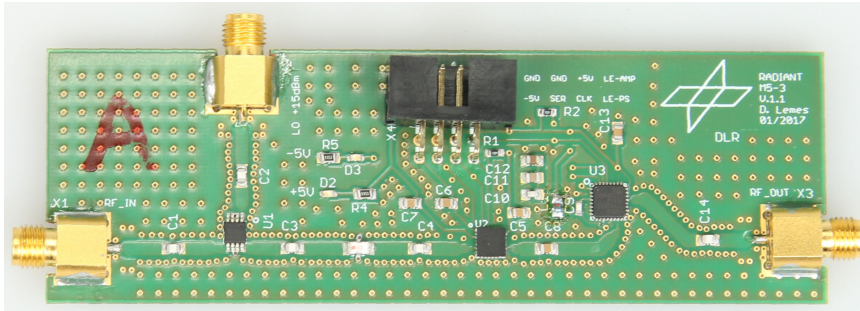
The components used in this work are listed in Table 10 along with the link budget of the combined transmitter. In this case, a C-band output signal around 7.0 GHz was generated from a 500 MHz input signal. Thus, the LO signals were chosen to be 1.4 and 5.1 GHz, respectively. The presented design shows a rather low gain of 6.4 dB. However, if larger output power is needed, this can be achieved by drop-in amplifiers or replacing the upconverter unit by a more powerful one.

The transmitter PCBs were fabricated using two-layer FR-4 substrate with standard

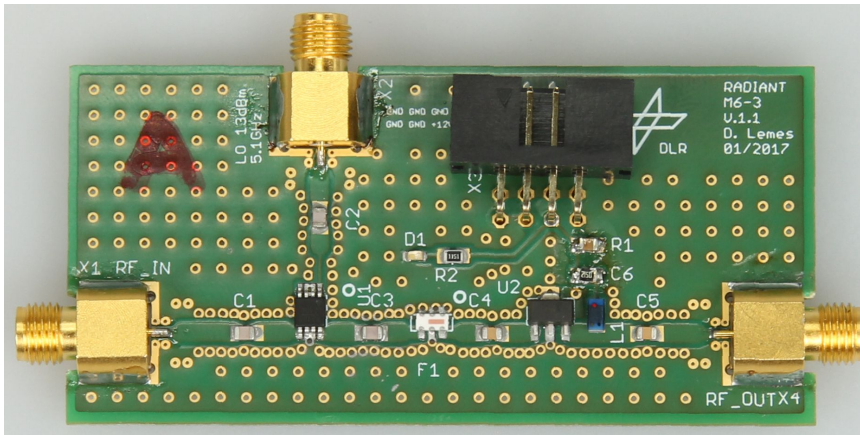


Table 10: Combined Link Budget

| Component   | Type          | Gain<br>dB | Budget<br>dB | Price<br>€ |
|-------------|---------------|------------|--------------|------------|
| HMC-316     | Mixer         | -7.5       | -7.5         | 6.07       |
| BFCN-1945+  | Bandpass      | -1.8       | -9.3         | 4.35       |
| MAPS-010163 | Phase shifter | -5.0       | -14.3        | 49.87      |
| ADL-5240    | VGA           | 19.7       | 5.4          | 7.39       |
| HMC-218     | Mixer         | -7         | -1.6         | 5.71       |
| HFCN-6010+  | Highpass      | -1.3       | -2.9         | 3.29       |
| GALI-2+     | Amplifier     | 14         | 11.1         | 1.27       |
| Total       |               |            |              | 77.95      |



(a)



(b)

Fig. 48: Assembled beamforming (a) and upconverter (b) PCB. The dimensions are 110 mmx36 mm and 74 mmx36 mm, respectively.

thickness of 1.55 mm. The cost for ten units, i.e. 20 PCB is currently around 180 €. The assembled circuits are shown in Fig. 48. Table 10 lists the price per piece for the RF components, Table 11 shows the prices of the additional parts of the transmitter. The prices are based on the assumption that a total of 10 transmitters is fabricated.

Table 11: Prices of Additional Parts

| Part                          | Unit price (€) |
|-------------------------------|----------------|
| PCB                           | 18.00          |
| SMA connectors                | 2.50           |
| Passive RCL components + LEDs | 15.60          |
| DC connectors                 | 0.60           |
| Total                         | 36.7           |

## 6.4 TEST AND MEASUREMENT METHODOLOGY

To assess the performance of the transmitters, two measurement techniques were used. First, standard vector-mixer calibration (VMC) using a vector network analyzer (VNA), an external LO, and a pair of calibration mixers is considered. This method is well suited to obtain the conversion gain of a single stage.

To perform beamforming, one needs the relative amplitudes and phases between all transmitters. This information was obtained by using the measurement setup depicted in Fig. 49 proposed in (LEMES; HECKLER; WINTERSTEIN, 2017). The transmitter input is thereby connected to the VNA port 1. The upmixed output signal is fed to two commercial mixers in downconverter configuration. The output of the second mixer is connected to VNA port 2. Two signal generators create the necessary LO signals, which are split and fed to the respective transmitter module and downmixer. Thus, the VNA can perform a normal S-parameter measurement whereby only S11 and S21 are of interest. All measurement devices are synchronized with a 10 MHz reference. The proposed setup can be used to calibrate the transmitters.

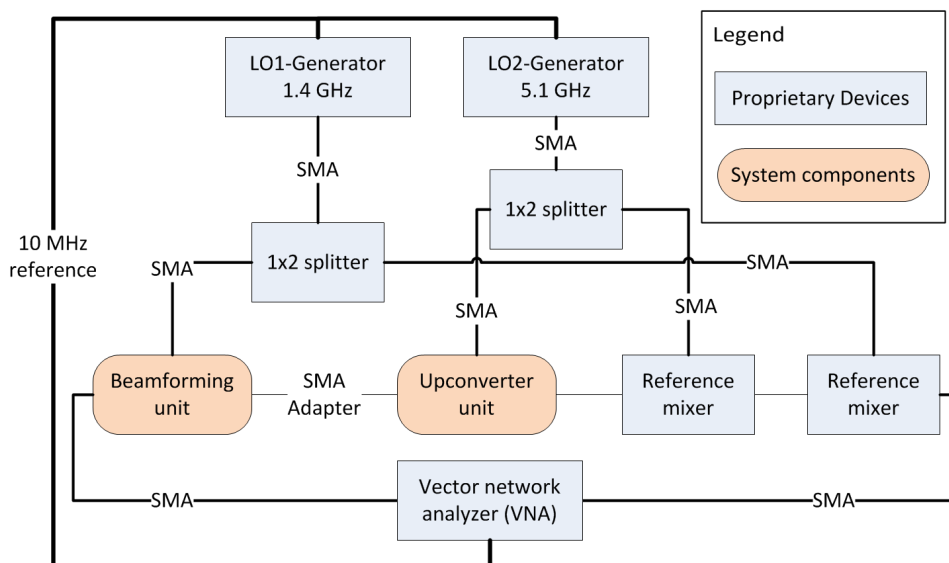


Fig. 49: Setup to measure the whole transmitter with a VNA.

## 6.5 MEASUREMENT RESULTS AND PERFORMANCE

The VGA and the phase shifter are 6-bit components, i.e. they have 64 possible levels. In order to preserve the visibility of the plots, only nine levels were plotted in each figure.

To prove the reproducibility, a comparison between three prototypes of the beamforming and upconverter modules is shown in Fig. 50 and Fig. 51, respectively. The small discrepancies between them are mainly due to the tolerances of soldering and the intrinsic variability of the electrical properties of the components. Based on that, the results of just one combined transmitter will be pointed out. This design turned out to present much more reproducible results than the previous transmitter design reported in (MAGALHAES, 2017).

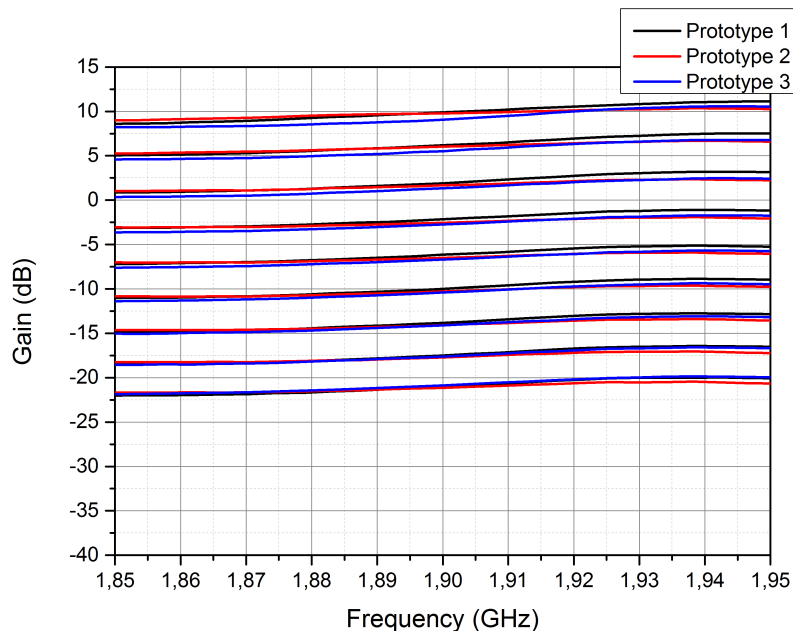


Fig. 50: Gain variation for 3 prototypes of the beamforming module.

### 6.5.1 BEAMFORMING MODULE

The following results were obtained using the standard VMC setup. Fig. 52 shows nine gain levels of the VGA. The phase variation capability of the beamforming module is shown in Fig. 53. Combining those two functionalities, it is possible to generate all coefficients needed.

During the measurements, a phase variation due to the operation of the VGA has been verified. By varying the gain level, different phase shifts have been measured even without changing the phase-shifter controlling bits. This occurs because the number of active attenuators present in the VGA changes for each gain level, which produces a



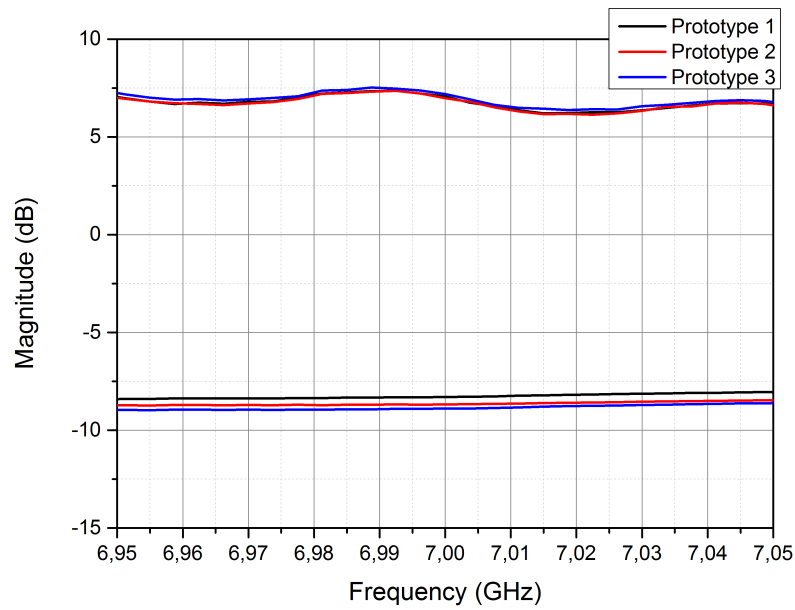


Fig. 51: S11 and VC21 for 3 prototypes of the upconverter module.

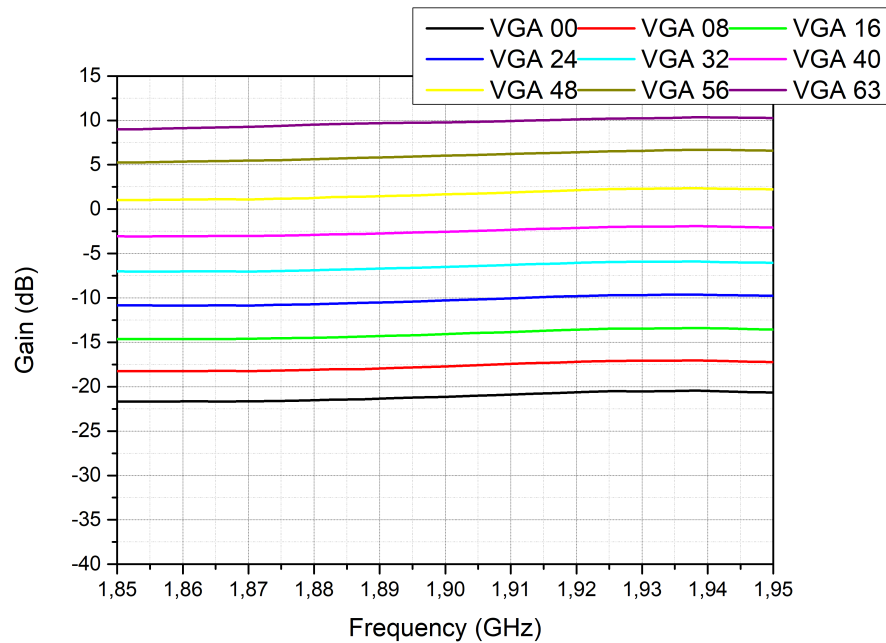


Fig. 52: Measured gain values for the beamforming module.

variation of the equivalent electrical length. Fig. 54 shows the phase introduced by the VGA by setting different gain levels. This difference is in a range of  $20^\circ$ . In order to increase the beamforming accuracy, this effect needs to be taken into account, i.e. a correction factor needs to be included in the calibration of the whole transmitter due to the presence of the VGA.

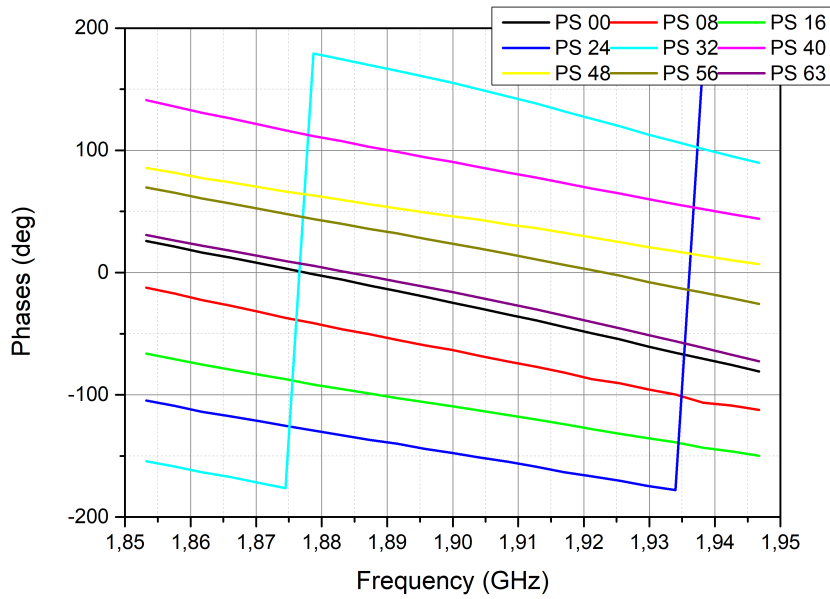


Fig. 53: Measured phase values for the beamforming module.

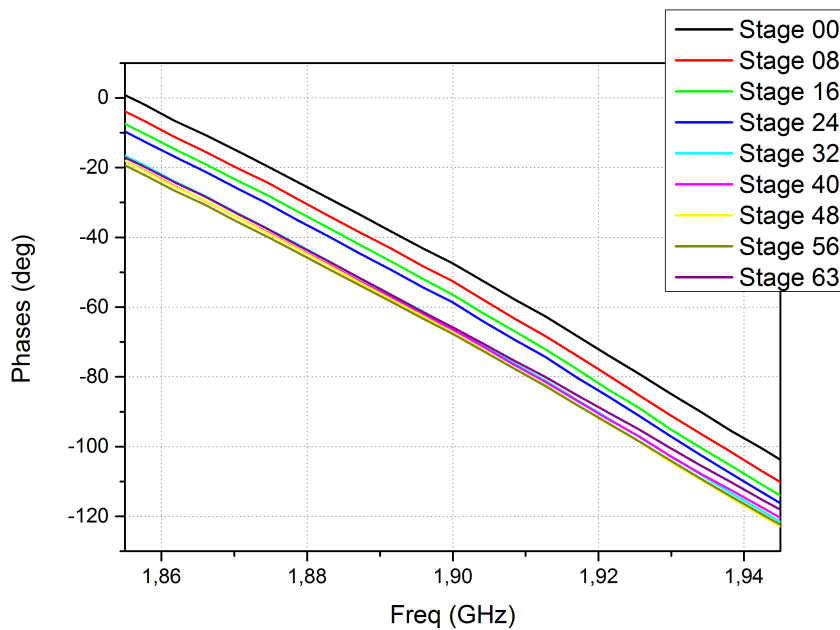


Fig. 54: Phase shift introduced by the VGA for different gain values.

After many investigations, it was noticed that the phase-shifter also inserts different gains i.e, each stage of the phase shift has a different gain. As occurs with the VGAs, this is mainly due to the different length of the lines and the number of diodes presents in the phase shifter. Fig. 55 shows the gain of the transmitter for different stages of the phase shifter.

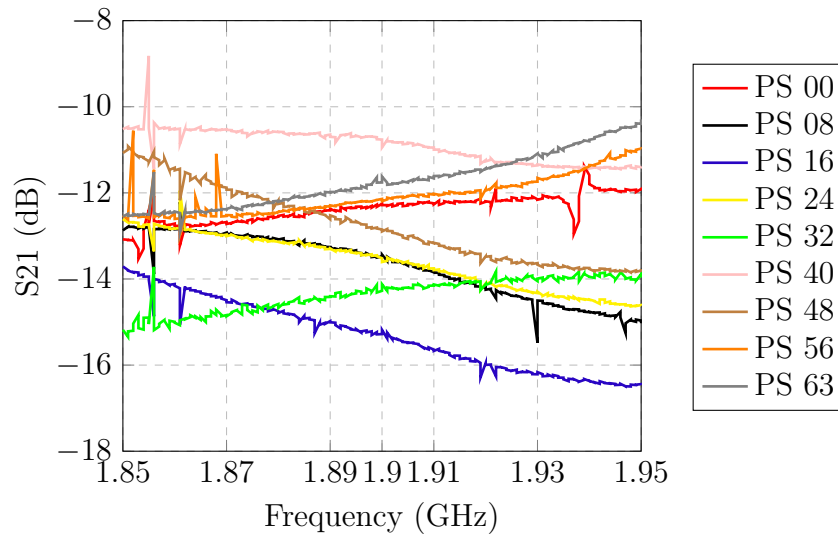


Fig. 55: Different insertion loss introduced by the PS for different phase values.

This effect, along with the effect inserted by the VGAs, has a huge influence on the measured patterns. A way to compensate this effect is by measuring all possible combinations between the phase shifter and VGA and then to insert the right stage of the phase shifter and VGA. However, there are 4096 combinations for each transmitter and it is impractical to do manually. For this reason, the use of the phase shifters and the VGAs was limited to perform the calibration, whereas the beamshaping is done directly in the digital domain (digital beamforming).

### 6.5.2 UPCONVERTER MODULE

Using again the standard VMC setup, the parameters  $S_{11}$  and  $VC_{21}$  have been measured and are shown in Fig. 51. These parameters show that the components have slight different insertion loss than it is given in the datasheet, but are still in an acceptable level. This module has a gain of 7.05 dB. The differences between the theoretical and measured gain are partially caused by the tolerances of the VMC calibration.

### 6.5.3 COMBINED TRANSMITTER

Using the proposed setup, the total gain and phase shift for both modules connected in cascade are shown in Fig. 56 and Fig. 57, respectively. These results show the capability of the combined transmitter to control the amplitude and phase of the output signal. The curves can also be used to calibrate the complete system, i.e to compensate the unbalances between different transmitters, which are caused by fabrication tolerances.

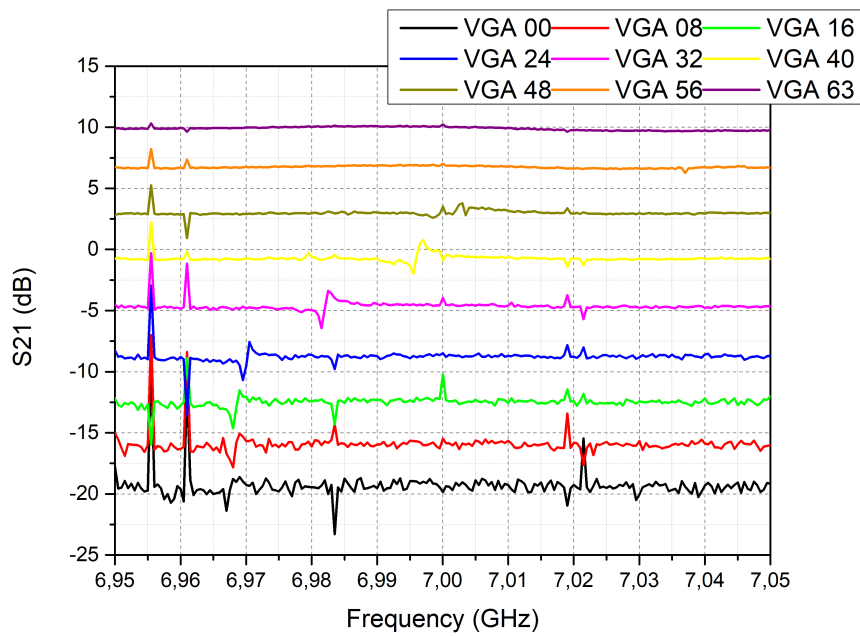


Fig. 56: Total gain for the complete transmitter controlled by the VGA less the losses introduced by the mixers.

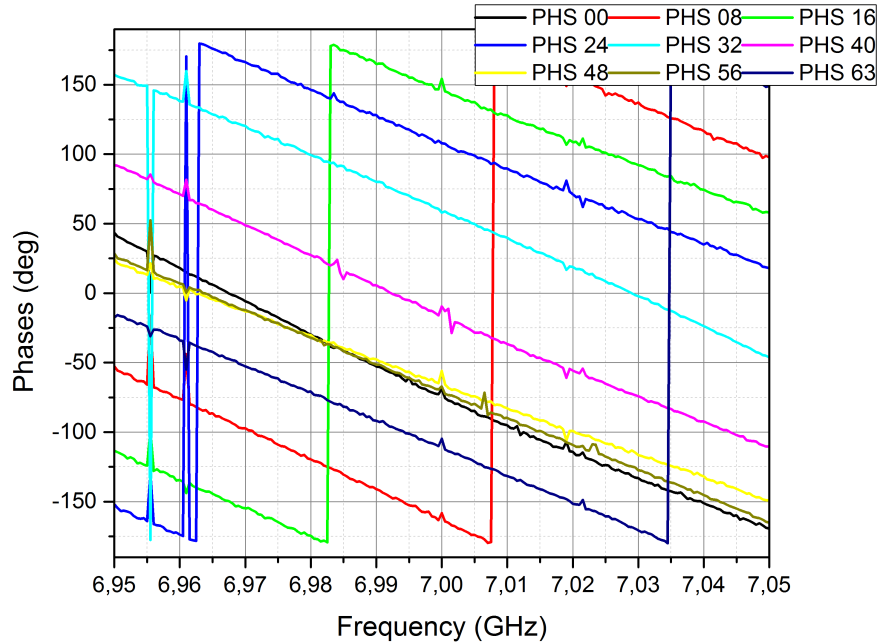


Fig. 57: Total phase shift for the complete transmitter controlled by the phase-shifter.

## 6.6 MEASURED PATTERNS

In order to test the functionalities and also its behavior when coupled to an antenna array, the designed transmitter has been applied to steer and to shape the main beam of

an eight-element linear microstrip antenna array. For this purpose, eight boards have been prototyped. Fig. 58 shows the fabricated boards during S-parameter measurements and calibration processes.

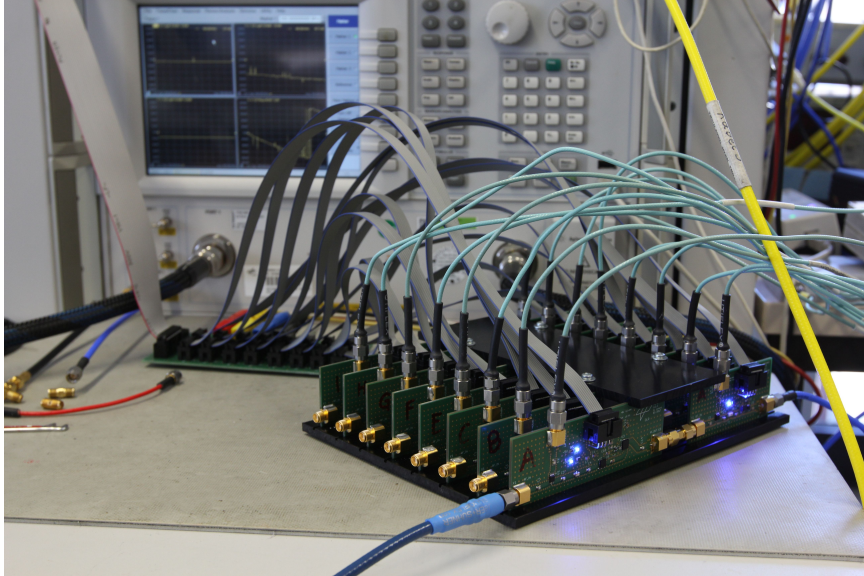


Fig. 58: Tests of eight channels of the proposed transmitter topology (Picture by Andreas Winterstein).

The used antenna array is a dual-band, dual-port, linearly polarized structure composed of eight patches resonating at 5.8 GHz and 7.0 GHz. The elements are equally spaced by half wavelength at 7 GHz. Since the output frequency of proposed transmitters is 7 GHz, only this frequency was used for the tests. The antenna array consists of two substrate layers glued with a ground layer between them to shield the antenna array from the feeder. The patches are rectangular and fed by vias that connected them to the feeding lines in the bottom layer. Fig. 59 shows the upper and bottom view of the antenna array prototype.

Fig. 60 shows the transmitter channels connected to the eight-element antenna array and all electronics and cables necessary to provide the needed voltages and to interconnect the FPGA to the VGAs and PSs.

Fig. 61 shows the whole integrated system combined installed for measurements in the anechoic chamber, with and without absorbers around it.

### 6.6.1 BEAMSTEERING USING THE PROPOSED TRANSMITTERS

Fig. 62 shows the measured radiation patterns for three different beamsteering conditions, where one can see that the main beam could be successfully steered to  $0^\circ$  (boresight),  $30^\circ$  and  $45^\circ$  with SLL control. From the measured patterns, one can see that



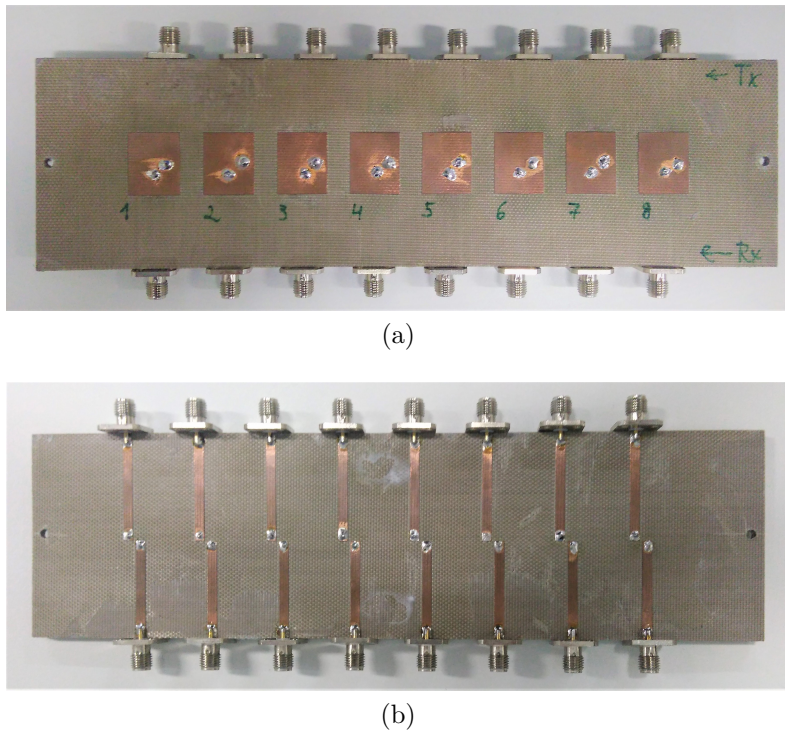


Fig. 59: Picture of the prototype of the antenna used: (a) Upper view; (b) Bottom view.

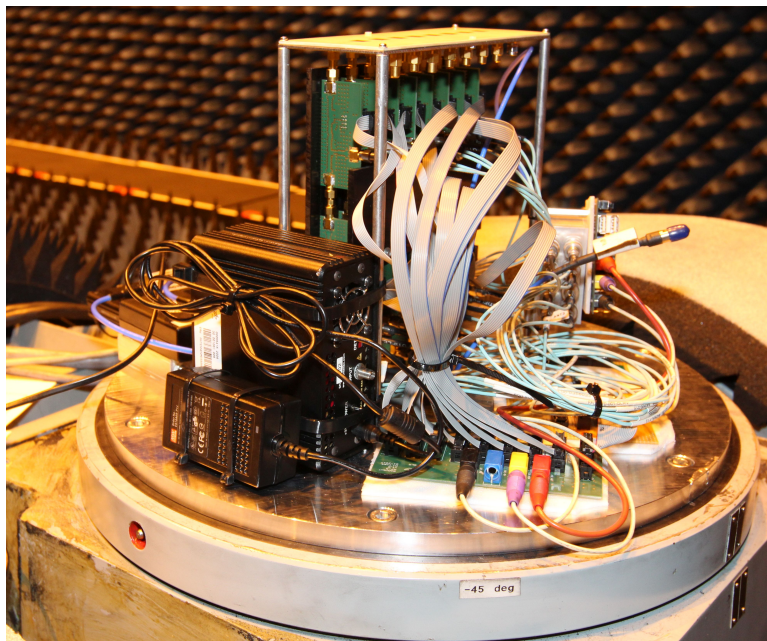
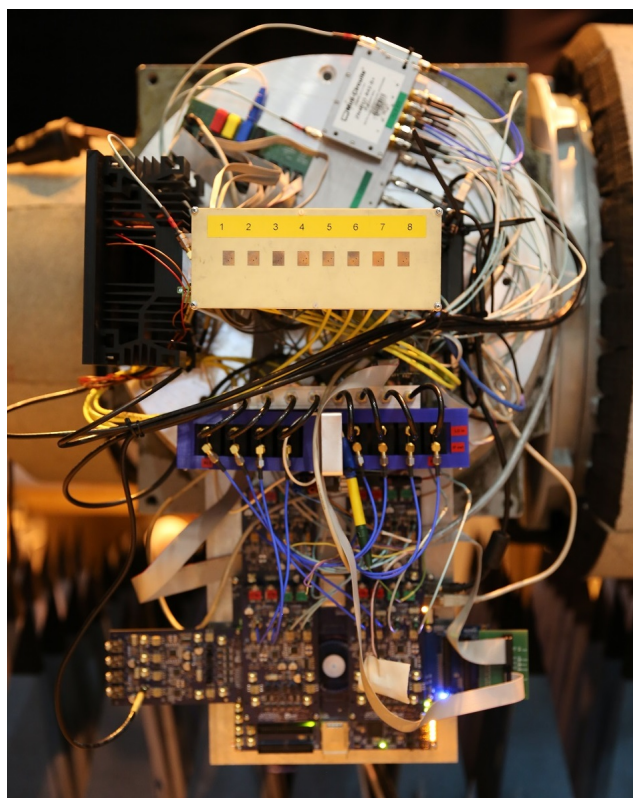


Fig. 60: Proposed transmitter connection with an eight-element antenna array (Picture by Andreas Winterstein).

the use of the proposed transmitter topology yielded acceptable experimental results. Table 12 shows the coefficients, calculated using PSO, for the three beamsteering cases.



(a)



(b)

Fig. 61: Picture of all system being measured in the anechoic chamber: (a) Without the absorbers; (b) With the absorbers. (Picture by Andreas Winterstein)



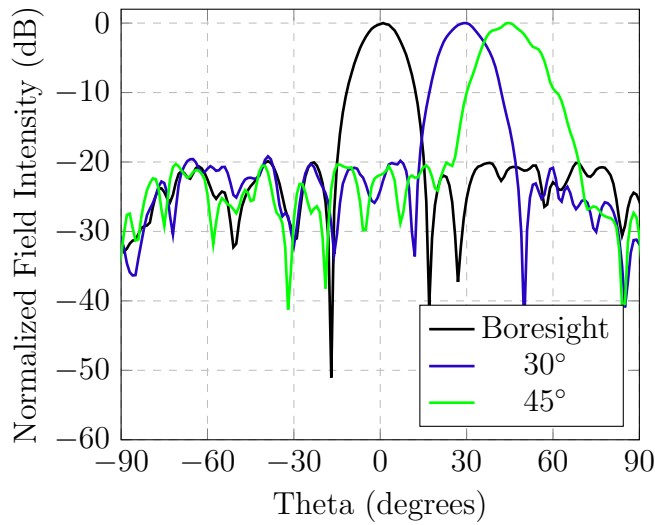


Fig. 62: Measured radiation patterns obtained with the proposed transmitter architecture of three beamsteering cases with SLL control.

Table 12: Coefficients of different steer angles calculated using PSO.

| Element                                     | 1      | 2      | 3      | 4      | 5      | 6      | 7      | 8      |
|---|--------|--------|--------|--------|--------|--------|--------|--------|
| <b>Broadside and SLL -20</b>                |        |        |        |        |        |        |        |        |
| Amplitude                                   | 0,45   | 0,48   | 0,75   | 0,85   | 1,00   | 0,62   | 0,68   | 0,41   |
| Phase (deg)                                 | 183,54 | 188,40 | 180,77 | 191,64 | 176,25 | 191,85 | 157,24 | 190,84 |
| <b>Steer angle equal to 30° and SLL -20</b> |        |        |        |        |        |        |        |        |
| Amplitude                                   | 0,40   | 0,57   | 0,56   | 0,78   | 1,00   | 0,69   | 0,54   | 0,59   |
| Phase (deg)                                 | 140,59 | 46,14  | 326,11 | 239,09 | 149,58 | 54,30  | 337,51 | 238,79 |
| <b>Steer angle equal to 45° and SLL -20</b> |        |        |        |        |        |        |        |        |
| Amplitude                                   | 0,47   | 0,77   | 0,71   | 0,80   | 1,00   | 0,97   | 0,77   | 0,55   |
| Phase (deg)                                 | 106,73 | 333,99 | 209,03 | 92,12  | 340,68 | 213,50 | 63,38  | 286,14 |

## 6.6.2 BEAMSHAPING USING THE PROPOSED TRANSMITTERS

In order to test the capability of the proposed transmitter to perform beamshaping, the radiation pattern was shaped following the squared cosecant contour and is shown in Fig. 63. The dashed red curve shows the mask previously described, the black curve shows the result using isotropic radiators to perform the optimization, the blue curve shows the resulting pattern by performing the optimization with the pattern of each element without the transmitters and the green curve shows the pattern using the pattern of each element with the transmitters coupled during the optimization. One can see the need to use the patterns of each element with the transmitter already coupled to perform the optimizations. This is mainly due to the coupling between the antenna array and the transmitters and by the transmitters with themselves and because of the small tolerances present in the components of the transmitters. One can notice, also, the importance to use the pattern of each element instead of isotropic antennas to perform the optimizations.



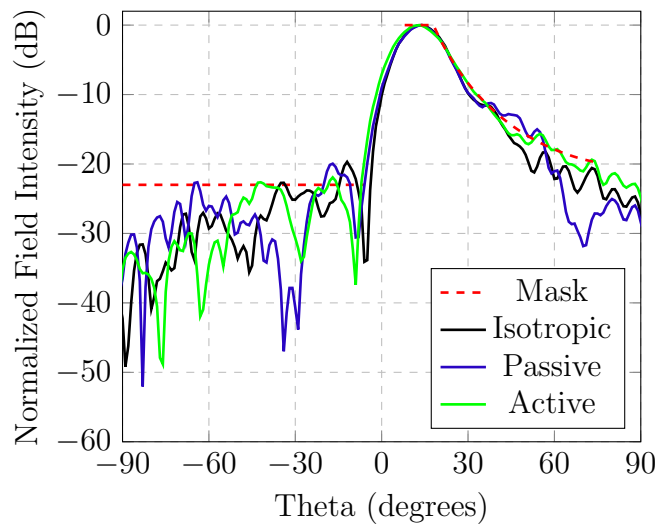


Fig. 63: Measured radiation patterns obtained with the proposed transmitter architecture by digital beamforming.

Table 13 shows the coefficients calculated using PSO to shape the main beam following the squared cosecant contour.

Table 13: Coefficients of cosecant squared beamshaping calculated using PSO.

| Cosec <sup>2</sup> using the pattern of the elements |        |        |        |        |        |        |        |        |
|--|--------|--------|--------|--------|--------|--------|--------|--------|
| Element  | 1      | 2      | 3      | 4      | 5      | 6      | 7      | 8      |
| Amplitude  | 0,10   | 0,22   | 0,30   | 0,80   | 0,75   | 0,98   | 1,00   | 0,55   |
| Phase (deg)  | 15,60  | 300,84 | 298,92 | 262,06 | 224,08 | 198,35 | 127,64 | 65,09  |
| Cosec <sup>2</sup> using isotropic radiators         |        |        |        |        |        |        |        |        |
| Amplitude  | 0,26   | 0,57   | 0,85   | 1,00   | 0,79   | 0,40   | 0,41   | 0,29   |
| Phase (deg)  | 100,13 | 55,43  | 364,47 | 312,68 | 261,41 | 218,95 | 214,58 | 153,61 |

It must be pointed out that the results shown in this and in the previous subsection have been obtained without any modification in hardware, hence demonstrating the flexibility of the proposed transmitter design.



## CONCLUSION

In this work, the main advantages of non-uniformly spaced arrays, such as the increase of degrees of freedom for the optimization of antenna performance, have been discussed. In order to optimize the amplitudes, phases and inter-element spacings of an antenna array, two optimization techniques were implemented and MATLAB-based codes have been developed. Taguchi's method has shown to be more robust because it has less parameters to be set and it is easier to be implemented than PSO. However, the latter provides, in general, better results provided that its parameters are correctly set. Both optimization techniques can be applied to optimize antenna arrays and are complementary. The codes proved to be useful in all investigations done. The optimization in Electromagnetics is not a simple process, so that there is no perfect technique able to achieve all desired goals. Thus, when available, more than one technique must be used and the best result should be chosen for implementation.

The proposed code was applied in the optimization of an array composed of dual-band dual-port antennas for base stations of mobile communication systems. Since the bands are well separated from each other, the main challenge was to obtain good performance in both bands, especially in terms of suppression of side lobes and grating lobes. Due to the larger electrical distance between the array elements in the higher band, the suppression of grating lobes could be only achieved by considering non-uniformly spaced arrays. The results show that the grating lobes can be well suppressed when the main beam has ordinary shape and points to the boresight in both bands. By implementing a squared cosecant shaped beam, the grating lobes could be partially suppressed in the higher band, whilst a pattern that fulfills all the specifications has been obtained in the lower band. Besides that, it was shown that performing optimizations with the embedded pattern of the center element of the array yields more accurate results because mutual coupling is partially taken into account in that case. Moreover, the optimization of spacings instead of amplitudes and phases has proven to be useful in order to obtain a simpler feeder network. All results were validated using the commercial software Ansys HFSS.

The proposed technique was also applied to synthesize a pattern with squared cosecant shape with a single-band antenna array for base station of mobile communication systems operating in the frequency band allocated for 4G/LTE services. The main objective was to reduce the number of array elements needed to realize the beam shape in comparison to previous work. In comparison to a uniformly spaced array, the number of elements could be reduced from 7 to 4 whilst fulfilling the specified pattern. Besides that, the importance of the social coefficient for this kind of problem was addressed. The impact of the mutual coupling into the synthesized pattern has been evaluated with the use of a commercial

software and the largest impact has been verified to occur in the region of the side lobes. It was also showed that it is possible to compensate the degradation inserted by mutual coupling by performing a new optimization of the amplitudes and phases. A passive feeder for this antenna array was also developed. The proposed array was prototyped and all conclusions were validated by measurements. Compared to the uniformly spaced array, the non-uniformly spaced array could be implemented with a much simpler feeder, lower cost and lower probability of failure, since it is composed of less elements. Besides that, the total dimensions have been also reduced.

A design scheme for an adaptive transmitter that performs analog and digital beamforming has been proposed. The use of a modular architecture with independent beamforming and up-converter units allows a flexible configuration in terms of transmit frequency and power. Additionally, the implementation of the proposed system operating in C-band was demonstrated, whereby very good performance and reproducibility have been verified. By using standard components and FR-4 laminates, the transmitter could be fabricated with low cost. A special setup was presented which allowed S-parameter measurements of the combined units. Finally, radiation pattern measurements demonstrated the beamforming capability of the proposed transmitter topology. With this technique, the total gain and the total phase shift produced by both designed modules could be characterized. This is a crucial information to implement the calibration and to perform beamforming accurately in a multi-antenna transmit system. During the development of the transmitter, the tests demonstrated that the place where the components are placed and also the number of vias influence on the results. In order to reduce the impedance from the ground pin of the components to the ground, some vias should be added as close as possible to the pins. All requirements were achieved, which means that a transmitter capable to change the level and phases of the signal and also to shift the frequency from 500 MHz to 7 GHz has been successfully developed.

As next steps, the proposed code can be extended for 2D planar antenna arrays. Another open point is the development of a method to compensate the undesired phase shift introduced by the VGA and the undesired insertion loss introduced by the PS in the transmitter chain. Furthermore, systematic investigations can be performed to assess clearly the influence of the inertia, parameter  $w$  on the convergence of PSO.

## BIBLIOGRAPHY

AL-KA'BI, A.; BIALKOWSKI, M.; HOMER, J. Mitigation of multipath propagation with the use of a non-uniform spaced adaptive array antenna. *Antennas and Propagation Society international Symposium (APSURSI) IEEE*, 2005. It was cited in 27.

ANSYS, C. Ansys hfss user's guide v.17. 2016. It was cited 7 times in pages 16, 32, 51, 52, 58, 59 e 62.

ATHLEY, F. Optimization of element positions for direction finding with sparse arrays. *Statistical Signal processing, Proceedings of the 11th IEEE Signal Processing Workshop on*, 2001. It was cited in 27.

BALANIS, C. A. *Antenna Theory Analysis and Design*. [S.l.]: John Wiley & Sons, 2005. It was cited 9 times in pages 15, 24, 31, 32, 33, 39, 40, 47 e 49.

BARBOSA, V. L. et al. Linear array design with switched beams for wireless communications systems. *International Journal of Antennas and Propagation*, 2015. It was cited in 29.

COMMISSION, F. C. Radio frequencies and their allocation. *National Radio News*, 1940. It was cited in 23.

ENACHE, F.; POPESCU, F.; DEPARATEANU, D. Multi-criteria optimization of non-uniform linear antenna array using genetic algorithms. *International Communications Conference (COMM)*, 2016. It was cited in 28.

FARIAS, R. L. *Antenas de Microfita Dupla-faixa para Aplicacoes em Estacoes Radio-base de Telefonia Movel Celular*. Dissertação (Mestrado) — Universidade Federal do Pampa, 2014. It was cited 4 times in pages 15, 39, 47 e 48.

FARIAS, R. L. et al. Dual-port dual-wideband annular slot antenna with stable unidirectional pattern. *Journal of Microwaves, Optoelectronics and Electromagnetic Applications*, 2018. It was cited in 47.

HSIAO, P.-C.; LIN, Y.-T.; CHEN, S.-G. An efficient searching algorithm for high dof non-uniform linear antenna array with constrained spacing. *Telecommunications (ConTEL), 13th International Conference on*, 2015. It was cited in 27.

JORGEN, J. H.; KAJ, M. Combined lp and quasi-newton method for minimax optimization. *Mathematical Programming*, n. 20, p. 49–62, 1981. It was cited in 28.

KAIFAS, T. N.; BABAS, D. G.; SAHALOS, J. N. A combined deterministic and stochastic approach for the design of non-uniform arrays. *7th European Conference on Antennas and Propagation (EUCAP) - Convened Sessions*, 2013. It was cited in 29.

KAWDUNGTA, S.; PHONGCHAROENPANICH, C.; TORRUNGRUENG, D. The mmm/ga design of non-uniform spacing collinear dipole antenna arrays. *Antennas and Propagation Society international Symposium (APSURSI) IEEE*, 2011. It was cited in 28.

- LEMES, D. L. et al. Analysis of dual-band non-uniformly spaced arrays for mobile communications. *Microwave and Optoelectronics Conference (IMOC) SBMO IEEE MTT S International*, 2017. It was cited in 49.
- LEMES, D. L.; HECKLER, M. V. T.; WINTERSTEIN, A. A low-cost modular transmit front-end with analog beamforming capability. *SBMO IEEE MTT S International Microwave and Optoelectronics Conference (IMOC)*, 2017. It was cited in 73.
- MAGALHAES, M. P. Design and analysis of an antenna array system for communication using high-altitude platforms. *Master thesis*, 2017. It was cited 4 times in pages 16, 67, 68 e 74.
- MALDAL, D.; DAS, S.; BHATTACHARJEE, S. Linear antenna array syntesis using novel particle swarm optimization. *Industrial Eletronics & Applications (ISIEA)*, 2010. It was cited in 36.
- QI-LI, G.; CHAO, S. Design broadband beamformer with constant beamwidth for non-uniform arrays. *3rd International Conference on Advanced Computer Theory and Engineering (ICACTE)*, 2010. It was cited in 27.
- ROBINSON, J.; RAHMAT-SAMII, Y. Particle swarm optimization in electromagnetics. *IEEE Transactions on Antennas and Propagation*, 2004. It was cited 5 times in pages 15, 29, 33, 34 e 35.
- SCHLOSSER, E. R. et al. Synthesis of linear antenna array for 4g mobile communication systems. *Microwave & Optoelectronics Conference (IMOC) SBM/IEEE MTT-S International*, 2013. It was cited 5 times in pages 16, 59, 62, 63 e 66.
- SCHLOSSER, E. R. et al. Synthesis and implementation aspects of linear antenna arrays with shaped radiation pattern for mobile communications. *IET Microwaves, Antennas & Propagation*, 2016. It was cited 5 times in pages 16, 43, 55, 60 e 64.
- STAHRIAN, S.; CHOI, Y.; ESHRAGHI, A. Antenna beam shaping using a non-uniform array antenna. *Recent Advances in Space Technologies, RAST 4th International Conference*, 2009. It was cited in 28.
- TACONIC. *Taconic, RF and Microwave laminates: TLC-338, datasheet, 2013*. [S.l.]. It was cited in 62.
- TELECOMMUNICATIONS, N.; COMMERCE, I. A. U. D. of. United states frequency allocations. *Office of Spectrum Management*, 2003. It was cited 2 times in pages 15 e 23.
- VARUM, T.; MATOS, J. N.; ABREU, R. Non-uniform microstrip antenna array for rx dsrc. *Antennas and Propagation Society international Symposium (APSURSI) IEEE*, 2014. It was cited in 27.
- WENG, W.-C.; YANG, F.; ELSHERBENI, A. Z. Linear antenna array synthesis using taguchi's method: A novel optimization technique in eletromagnetic. *IEEE Transactions on Antennas and Propagation*, 2007. It was cited 5 times in pages 18, 29, 36, 37 e 38.

## **Appendix**





## A IMPLEMENTATION ISSUES OF THE STUDIED OPTIMIZATION TECHNIQUES

As discussed in the main part of this work, some optimization technique must be used to find the best values of amplitude, phase and relative spacing of each element of a non-uniformly spaced antenna array in order to synthesize the desired pattern. Based on that, the two optimization techniques described in chapter 2 were implemented in MATLAB and the main implementation issues will be pointed out in the next sections.

### A.1 SETTING UP THE MASK

In order to develop a code capable to deal with different applications, the implementation was done based on the fact that there are many goals that must be fulfilled by changing the complex excitation coefficients and spacings. If it is physically possible, the code enables to optimize the following properties:

- To shape the main beam;
- To achieve a desired directivity;
- To insert nulls in the radiation pattern;
- To steer the main beam;
- To control side lobe level (SLL);

To cover all these possibilities, a mask must be generated prior to running the optimization routine. A mask is a file that contains the goal of the optimization, i.e, it will be used to evaluate how close the algorithm is to fulfill the optimization criteria.

The format “xlsx” (MS Excel) for the mask was chosen in order to facilitate the construction of the mask, since it is possible to see graphically what is built up. In the file, there are four columns: the first one is used to define the angular region for the optimization. It has been fixed from -180 to 180 degrees. The second column contains the desired levels, in dB, for each angle. The third column stands for the weights that are used to set priority to the goals. For example, if the goals are to steer the beam and to control the SLL, then, using the weights, it is possible to set priority in one of the two goals. Finally, the fourth column contains the information if the pattern level must be below (-1) or above (1) the level specified in column 2, or must follow a given contour (0). When 0 is set, a tolerance option can be added. This allows to relax the requirement to follow the mask for the cases where other goals cannot be achieved.

A special feature of the mask is the inclusion of priority to optimize a specified region of the pattern (weights). Besides that, the way how the weights are chosen has a high influence on the final result of the optimization process, as expected, hence the choice of the weights must be done carefully.

Fig. 64 shows a mask along with the respective data table for the case of a main beam following a squared cosecant contour from  $8^\circ$  to  $77^\circ$  with simultaneous side lobe level suppression in the angular ranges of  $-180^\circ$  to  $-6^\circ$  and  $78^\circ$  to  $180^\circ$ .

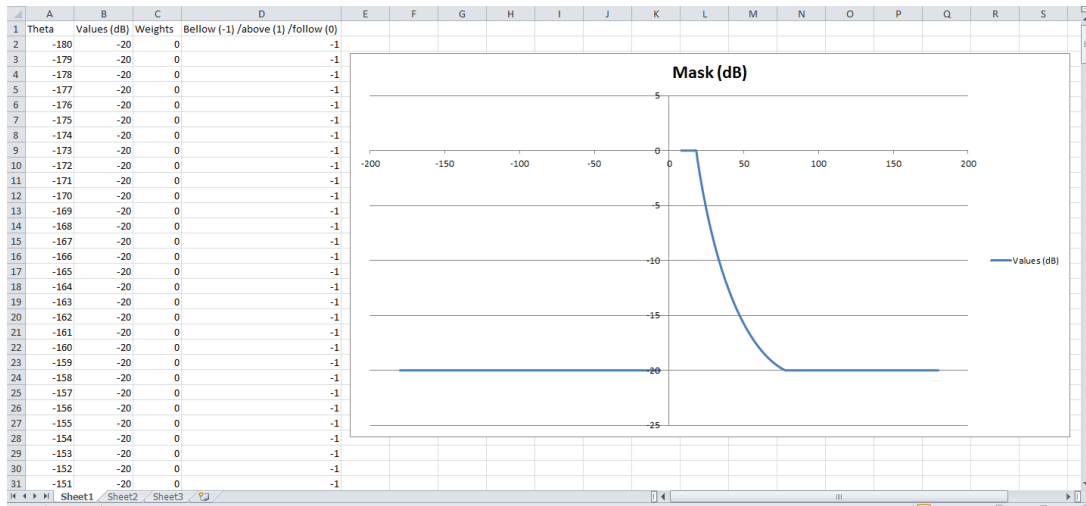


Fig. 64: An example of mask where from  $-180^\circ$  to  $-6^\circ$  and from  $78^\circ$  to  $180^\circ$  the pattern must be below the mask and from  $8^\circ$  to  $77^\circ$  it must follow the mask.

## A.2 IMPLEMENTATION ISSUES OF THE OPTIMIZATION ROUTINES

One can see that the developed code is as general as desired and allows many possibilities, which enable the user to:

- Optimize amplitudes, phases and relative spacings of each element in an antenna array;
- Optimize all permutations of those parameters;
- Optimize patterns with or without normalization;
- Optimize amplitude and phases importing the pattern of each element, taking into account mutual coupling for a predefined array geometry;
- Apply penalties for the correct positioning of maximum directivity;
- Optimize linear arrays with any number of elements;
- Set the maximum number of iterations.

Two MATLAB-based codes were developed with the same structure and options, but with different optimization techniques: PSO and Taguchi's method. Fig. 65 shows the flowchart of the codes.

The "mutual coupling" option allows to choose if the code will import the embedded pattern of each element of the array or just the pattern of one single and isolated element. This option was created because it is possible to simulate an array, using a commercial software, and export the pattern of each element taking into account the mutual coupling. If this option is enabled, the code imports automatically all patterns and only amplitudes and phases can be optimized, since each pattern was extracted for a given array geometry with fixed set of spacings.

Another option allows the user to work with normalized patterns. This was included because, after many optimizations, it was realized that, when beamshaping is needed, the maximum directivity may influence the optimization process. In other words, when a mask is built and beamshaping is required, the selected directivity affects the shape of the pattern. This is an undesired effect, since, for many cases, the format is more important than the directivity itself.

It is also possible to optimize amplitude, phase and spacing alone or any permutation between them (including all three). There are cases where the pattern fulfills the mask whilst the main beam points to a slightly different direction compared to the desired one. Because of that, the option to include a penalty in the fitness function when such cases occur was created.

It is known that many iterations are needed in order to choose the correct weights, to choose which goals are physically possible, etc. After each iteration, the code creates a .txt file which contains the number of iterations, the time of the optimization, the residual error, the optimized magnitudes, phases and spacings, the angles, mask and the optimized directivity.

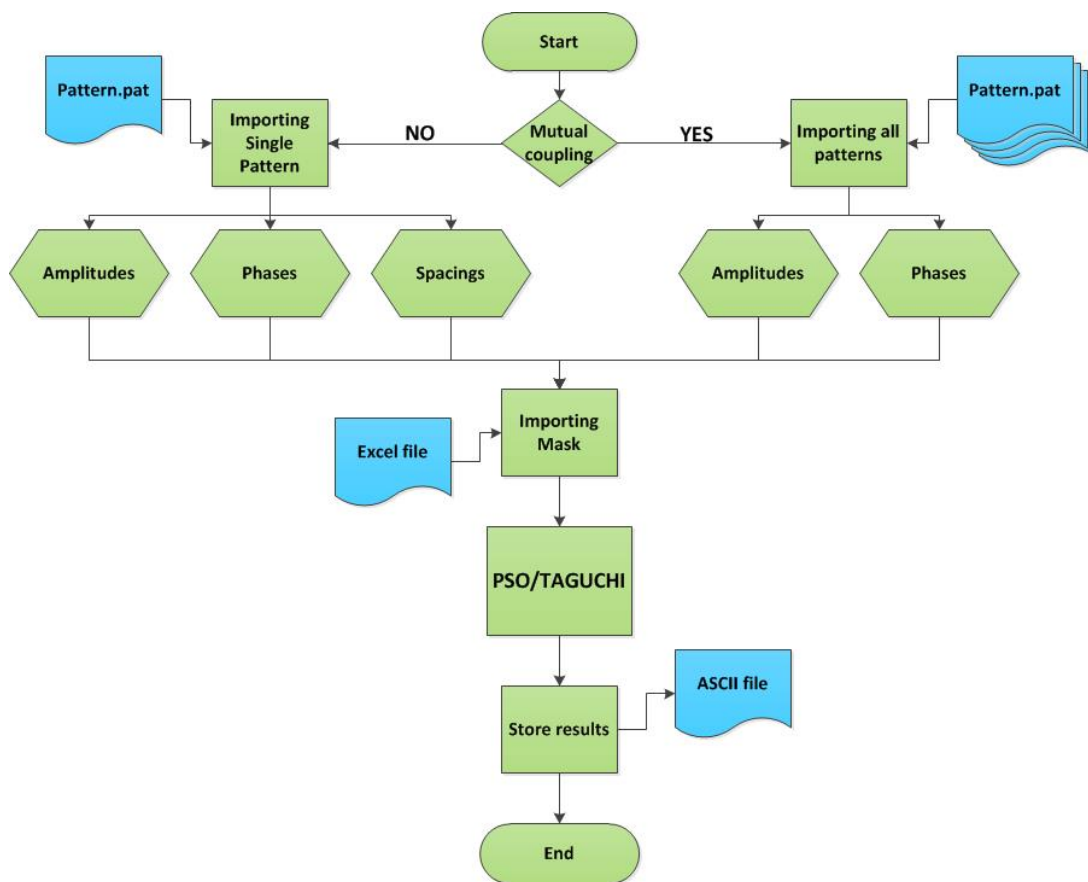


Fig. 65: Flowchart used for the implementation of both optimization techniques.